Delft University of Technology

Bachelor Thesis
AESB3400

2D Modelling of a fold and thrust belt in the French Prealps

Author
F.J.J. Smit

Student number
4483685

Supervisors
Jan Kees Blom
Karl-Heinz Wolf
Pierre-Olivier Bruna

April 11, 2020

Abstract

During this thesis, 2D modelling using the MOVE software suite is performed on a fold and thrust belt in the French Prealps. The area of interest is called the *Couspeau* area and is 72 km^2. In this area, Vocontian basin sediments deposited during the Jurassic and Cretaceous can be found. The area contains well exposed fold and thrust structures. The oldest structures begin in the West, while the younger ones can be found in the East. All thrusts strike approximately N-S. These thrusts were assumed to be formed by the second Alpine orogeny.

A structural map of the area was created in QGIS version 3.12.0 using geologic maps from the BRGM and using fieldwork data from Applied Earth Sciences students collected during the AESB2430 course at TU Delft. Subsequently, four E-W orientated cross sections of the area were constructed. These sections were restored using MOVE to verify if the interpretations were geologically feasible. 2D forward modelling was then applied to discover possible types of structural mechanisms which were active in this area. Possible mechanisms include fault-bend folding and regular folding. Fault propagation folding was assumed to be a suitable mechanism, but didn't produce satisfactory forward models. Strain circles were added during forward modelling to analyse what kind of deformation is caused by different thrusting mechanisms.

The restored sections were also used to calculate the total amount of shortening in the area, and how much of this shortening was caused by folding or faulting. The total amount of shortening was 24%, from which 38% was caused by faulting and 62% by folding.

Contents

1 Introduction

The goal for this thesis is to use 2D forward modelling to discover what kind of structural mechanisms were possibly active in the area of interest. The secondary goal is to determine how much overall shortening was caused by these mechanisms. By researching these two subjects a better understanding of the structural evolution of the area could be obtained. Understanding of such structural evolutions plays a vital role in predicting locations of subsurface resources, help manage risks of volcanism, earth quakes and slope failure and help understand larger scale processes like mountain building.

During forward modelling, strain circles were included in the examined formations. The shape of the deformed circles contains information on how the deformation occurred (Fossen, 2010), and provide a visualisation of how the structural mechanisms deformed the examined formations. An extensive study on 2D forward modelling and strain development in a fold and thrust belt in Scotland was done by Watkins, Butler, Bond, and Healy (2015). They used 2D forward modelling to determine strain distribution throughout the folds in order to determine the influence of structural position on the formation of fracture networks.

The area of interest for this thesis is named the *Couspeau* area. This is an area of 72 km^2 and is named after the Couspeau mountain. The area lies within the French Drôme department. Drôme is situated in the French Prealps, located West of the French Alps. Figure 1.1. A couple of well exposed fold and thrust structures can be found in the Couspeau area, thus it provides a good location for discovering by what mechanisms these structures were formed.

For this thesis, four balanced, E-W orientated cross sections were constructed in the area of interest. Section restoration was performed on these sections to check whether they were balanced. The sections were restored and forward modelled using the Petex MOVE software suite. In order to make these cross sections, first a topography profile was created in 3D using a DEM file in MOVE. Second, a geologic structural map was draped on top of the profile. The structural map was created in QGIS version 3.12.0, using geological maps from the Bureau de Recherches Géologiques et Minières (BRGM). Data collected by students during the AESB2430 course have been used as well. Using the maps and data, 2D cross sections could be sketched and digitized.

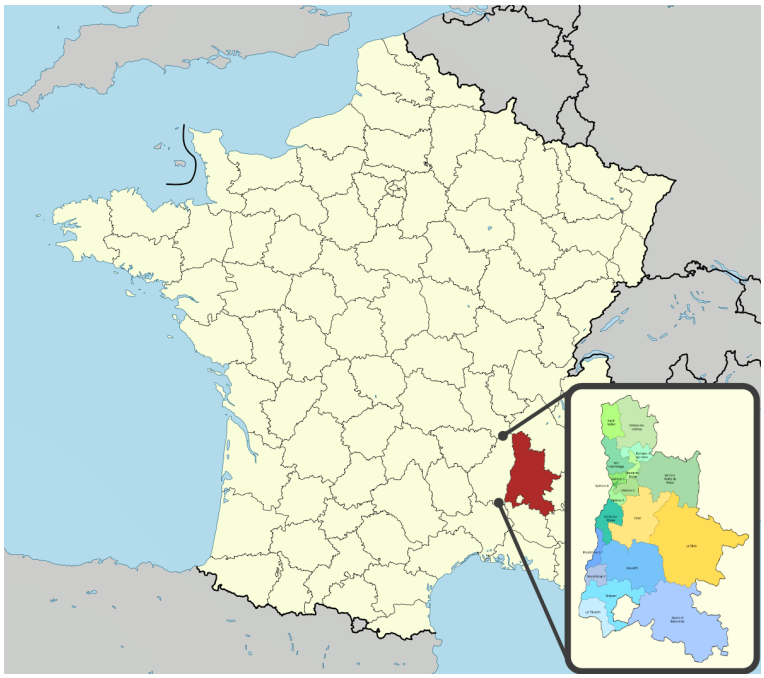

(a) Location of the Drôme department on the map of France

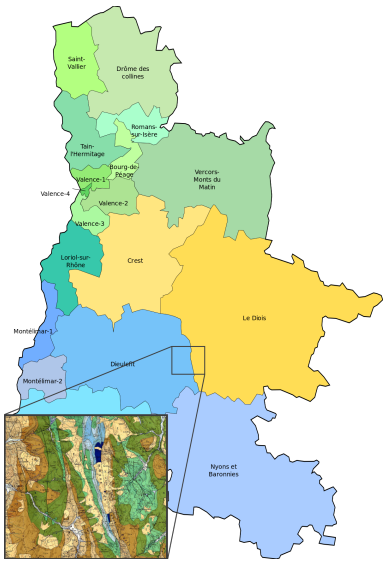

(b) Location of the Couspeau area

Figure 1.1

2 Geological history

In order to understand the present-day geology in the region of interest, an understanding of the geological history is needed. Therefore the subchapters describe the creation and filling of the Vocontian basin and the deformation of the area due to orogenic phases. These events cover the period from the Mesozoic up until the present.

2.1 Creation of the Vocontian basin

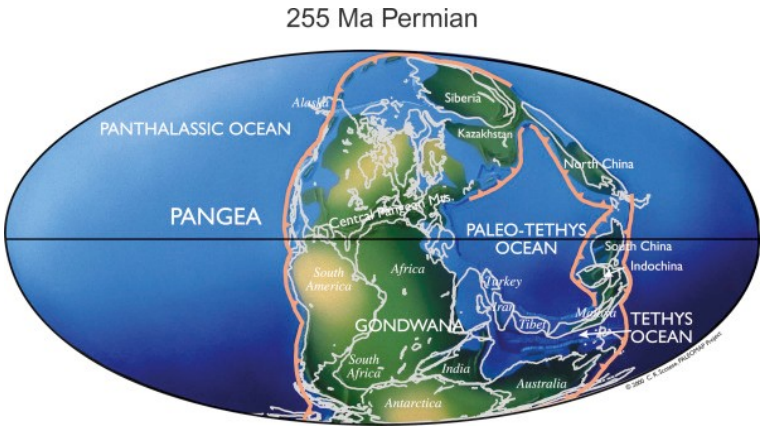

Figure 2.1: Pangea during the Permian (Henderson et al., 2012)

The supercontinent Pangea, which formed during the Paleozoic, started to break apart during the Triassic (Hallet & Clark-Lowes, 2016). The break-up of the supercontinent marked the start of the rifting phase of Laurasia and the eastward rotating of Gondwana. The rifting started the formation of many shallow seas in between the land masses, which were later connected due to the sea level rise in the Triassic (Boulila, Galbrun, Hinnov, & Collin, 2008), (Bombardiere & Gorin, 2000). In the Early Jurassic this rifting of Gondwana and Laurasia continued (Lemoine et al., 1986). This extension led to the Early Cretaceous opening of the central Atlantic Ocean and consequent break-up in the Alpine Tethys, which led to the creation of the Vocontian basin (Stampfli & Borel, 2002), (Bruna et al., 2013). This basin was a gulf, shaped like a horseshoe, with an opening to the east and surrounded by the Jura and Provence carbonate platforms (De Graciansky & Roberts, 2011).

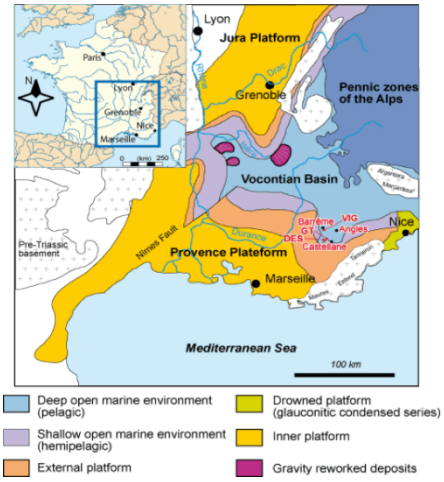

Figure 2.2: Paleogeographic map of the location of the Vocontian basin during the Jurassic (Arnaud, 2005)

2.2 Filling of the Vocontian basin

During the Jurassic and Cretaceous, the Vocontian basin was filled up with sediments. The formations examined during this thesis were deposited in this basin from the Late Jurassic to Early Cretaceous. In order to better understand their structural behaviour, it is important to describe the content and depositional conditions of these formations. The basin was filled by pelagic sediments and sediment brought to the basin from the surrounding carbonate platforms and continents laying behind them (Colombié & Strasser, 2003). The package contains alternating marl and limestone deposits. For this thesis, the package is subdivided into 5 groups. This division into groups was implemented to keep clarity and leave out negligible details. All grouped formations have common depositional characteristics. The names of these groups were derived from the ages in which they were deposited.

The first group was deposited during the Late Jurassic and is named the *KimArgOx* unit. This unit contains carbonate rich marls due to the pelagic setting in the basin during the Jurassic (Boulila et al., 2008). The second group is the *Tithonian* unit, deposited at the end of the Jurassic. The Tithonian is an almost pure limestone formation. Practically no clay is found in this formation, due to further sea level rise (Colombié & Strasser, 2003). The next group is the *HautValBerr* unit, deposited during the start of the Cretaceous. During this period, there were many climate oscillations. Sea level fell and rose in relatively quick succession (Föllmi, 2012). Therefore this unit is characterized by regularly alternating bands of limestone and marl. The following group is the *Barremian* unit. The Barremian is a formation composed of mostly limestones deposited by turbidic events. During the Barremian age, sea level had rose again, leading to the deposition of carbonate rich sediments (Föllmi, Godet, Bodin, & Linder, 2006). The last group is the *Albian/Aptian* unit. During this time, terrigenous-dominated sedimentation occurred, which led to a formation consisting of mostly marls (Caillaud et al., 2020).

2.3 The orogenic phase

After a long period of extensional rifting during the Late Jurassic-Cretaceous, a period of shortening occurred. During the Cenozoic, continents which were formally part of Gondwana collided with the Eurasian continent (Wan et al., 2019). The whole area, including the Vocontian basin, was uplifted during the Eocene and Oligocene. During this period, two Alpine orogenic episodes are defined. First of all, during the Eocene, the first Alpine orogeny commenced causing a N-S shortening (Dumont et al., 2012). This event is linked to the Pyrenean orogeny (De Graciansky & Roberts, 2011). This lasted until Early Oligocene, when the next episode commenced. The second Alpine orogeny caused E-W orientated shortening and was therefore almost perpendicular to the previous phase. It was caused by the westward movement of the Adriatic plate during the Oligocene collision stage (Dumont et al., 2012). N-S striking faults and folds in the Couspeau area were created by this event. Since faults and folds with a N-S strike are dominant in this area, the second Alpine orogeny is interpreted to be the main force which created these structures. See Figure 3.3a.

3 Present-day geology

The present-day geology of the Couspeau area is important to analyse because it provides insights in the structural evolution of the area. subsection 3.1 describes where the units defined in subsection 2.2 come to the surface and how this relates to the elevation profile of the area.subsection 3.2 describes some geologic structures found in the area, where they are located and some theories are provided to how these structures were formed.

3.1 Locations of surfacing formations

The dominant ridge in the Couspeau area is the Couspeau mountain. This ridge runs from North to South, through the middle of the area and divides the area roughly into two compartments. The Titonian formation can be found at the top of the ridge. Since the Titonian consists of pure limestone bands (subsection 2.2), is it the hardest formation in the area and therefore responsible for creating the highest ridge. Several smaller ridges are situated in the East and West compartments. The Barremian formation is, like the Titonian, a limestone rich formation and can therefore be found on top of these ridges. The HautValBerr and KimArgOx units are not as hard as the Titonian and Barremian formations, due to their alternating limestone and marl bands (subsection 2.2), and are therefore found on the mountain slopes and in the valleys (Figure 3.1a). The Albian/Aptian unit consists of soft marls (subsection 2.2) and is therefore mostly found in the valleys (Figure 3.1a).

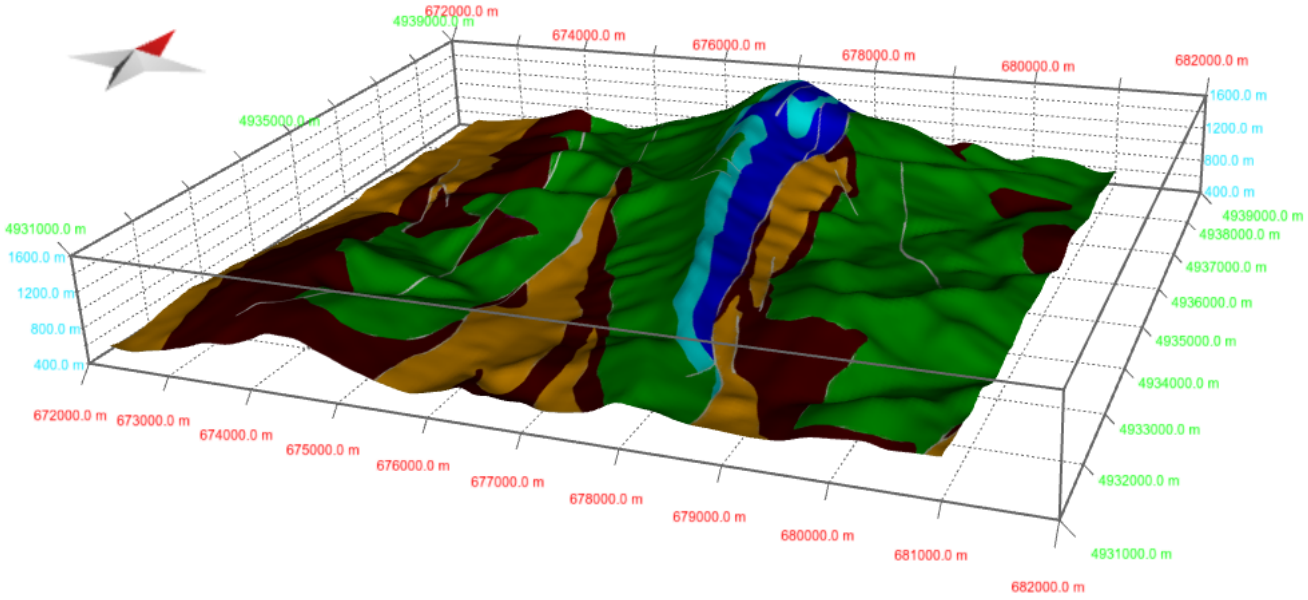

(a) DEM with draped geologic map

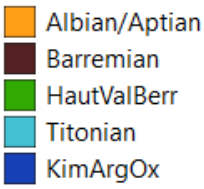

(b) Legend

Figure 3.1

3.2 Structures

The area is dominated by thrust faults, as can be seen in Figure 3.3a. These faults are all dipping to the West. The layers were displaced in East direction, creating thrust faults and folds striking N-S. The oldest faults can therefore be found in the West and they become younger to the East. This indicates that the major stress direction originates from an E-W shortening episode. This episode is assumed to be the second Alpine orogeny (see subsection 2.3). Many folds are situated right next to faults (Figure 3.3a). This indicates that much of the folding in the area was caused by faulting. There are several possible thrusting mechanisms which could be responsible for creating these folds. The mechanism that is mostly used in this thesis is the fault-bend fold method. This method creates folds which geometry is parallel to the fault surface in the backlimb and steeper dipping in the forelimb, as shown in Figure 3.2a (Fossen, 2010). Another viable option is the fault-propagation fold method. With this method folds are formed in front of a propagating fault tip (Fossen, 2010). The blacklimbs of the fault propagation fold are positioned parallel to the fault surface, but at the forelimb the layers are overturned to a almost 90^o angle, creating a much more asymmetric fold compared to fault-bend folding. See Figure 3.2b.

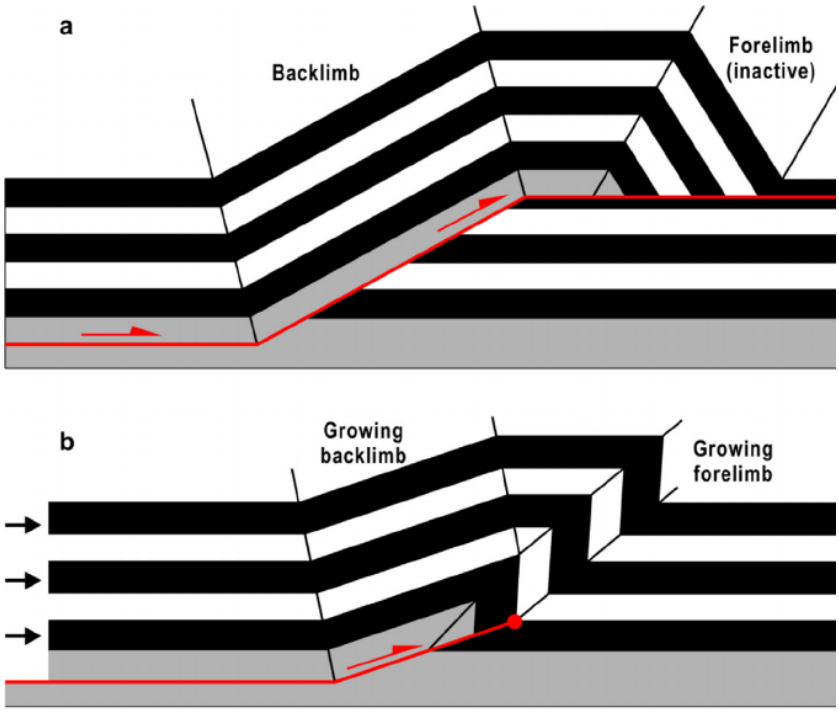

Figure 3.2: a) Fault-bend fold b) Fault-propagation fold (Pei et al., 2014)

Most of the layers in the area are dipping towards the West (Figure 3.3a). Cross sections made of the area suggest the same (Figure 4.6, Figure 4.7, Figure 4.8, Figure 4.9). However, anticline A6 striking N-S and running close to the SN fault (Figure 3.3a) causes layers to dip to the East in the East part of the area.

Two synclines, S3 and S4 strike N-S, East of the CE fault (Figure 3.3a). These synclines are separated by a narrow Barremian outcrop. This is probably an relay structure formed between the two folds.

The last highlighted structure is found at the Northern end of the Couspeau mountain. It can be observed in Figure 3.1a and Figure 3.3a that the Couspeau ridge has a small width at the top due to the thin Titonian formation surfacing here. However, this changes in the North. Here the peak is much wider. This is due to a small fault which branched of the CE fault. This fault tilts the otherwise steep dipping Tithonian formation to a more horizontal position. Due to this, the peak is a few hundred meters wider.

The dip angle of the faults in the Couspeau area are very steep (see subsection 4.3). This could be due to the faults having a long, listric geometry. They start out relatively flat, but when they come close to the surface, they take a shortcut due to the smaller load of the overlying sediments. The result is a fault with a steep dip close to the surface (Amos, Burbank, Nobes, & Read, 2007). It should be noted that this is only a hypothesis and doesn't necessarily define the actual situation.

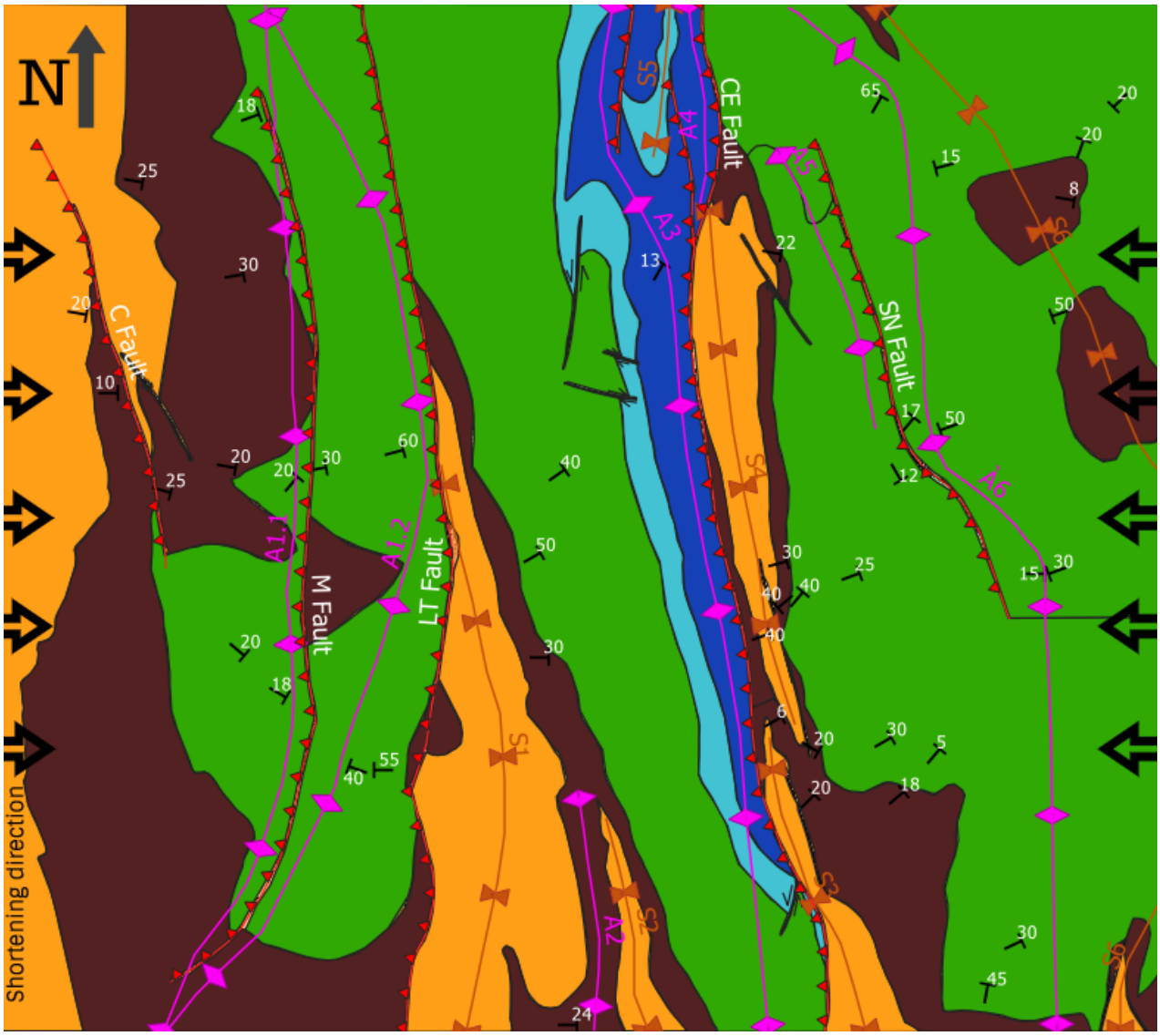

(a) Structural map of the Couspeau area. The names of the faults and folds are not the official names

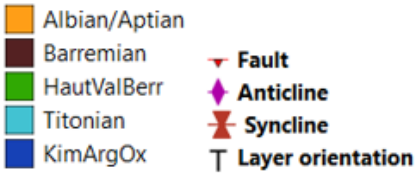

(b) Legend

Figure 3.3

4 Data acquisition

4.1 Field data

During the second year of the bachelor Applied Earth Sciences at TU Delft, students travel to the late Vocontian basin area to practice geologic mapping in the field. Data from four groups of students who worked close to the Couspeau area have been used during this thesis. Figure 3.3a shows the measured dip directions with associated dip angle.

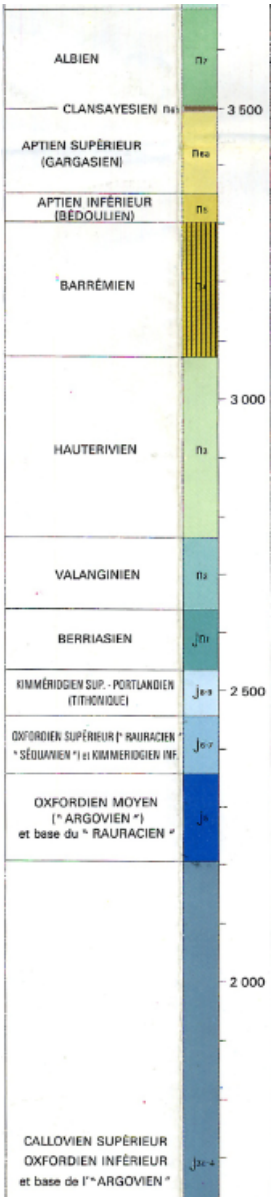

Figure 4.1: Stratigraphic column from the Nyons map (BRGM, 1975)

To determine the bedding thicknesses of the five grouped formations, geological maps from the Nyons and Die areas were consulted. These maps provided stratigraphic columns which contained the bedding thicknesses of the formations of interest (Figure 4.1). The final determined thickness for each formation group is shown in a table in Figure 4.2.

The detachment surface was calculated by using the Epard and Groshong method, as described by Li, Feng, Tang, Rao, and Bao (2009). The average from all cross sections showed a detachment at about -2700 m depth. At this depth the Banthonian formation can be found. This is a soft formation consisting of marls and clay (BRGM, 1974). For simplification reasons, the detachment surface was assumed the be constant and horizontal in the whole area.

Formation	Thickness (m)
Albian/Aptian	200
Barremian	150
HautValBerr	500
Titonian	75
KimArgOx	1400

Figure 4.2: Thicknesses of formation groups

4.2 Digital data

From a geological map of the Dieulefit area, the Couspeau area was clipped (BRGM, 1969). The clipped map was geo-referenced using QGIS. The coordinate boundaries used for geo-referencing can be found in Figure 4.3. Using the clipped map, a new geological map was created in QGIS, showing only the five grouped formations. Next, a topographic profile was loaded in MOVE using a DEM file of the area. From this profile, the area of interest was also clipped by using the coordinates from Figure 4.3. The new geological map was then draped on top of the clipped profile (see Figure 3.1a). Doing this first made it easier to construct cross sections.

North	44°45'10.44
South	44 ° 37'90.44
West	6 ° 04'80.06
East	6 ° 12'90.06

Figure 4.3: Coordinates of the area boundaries

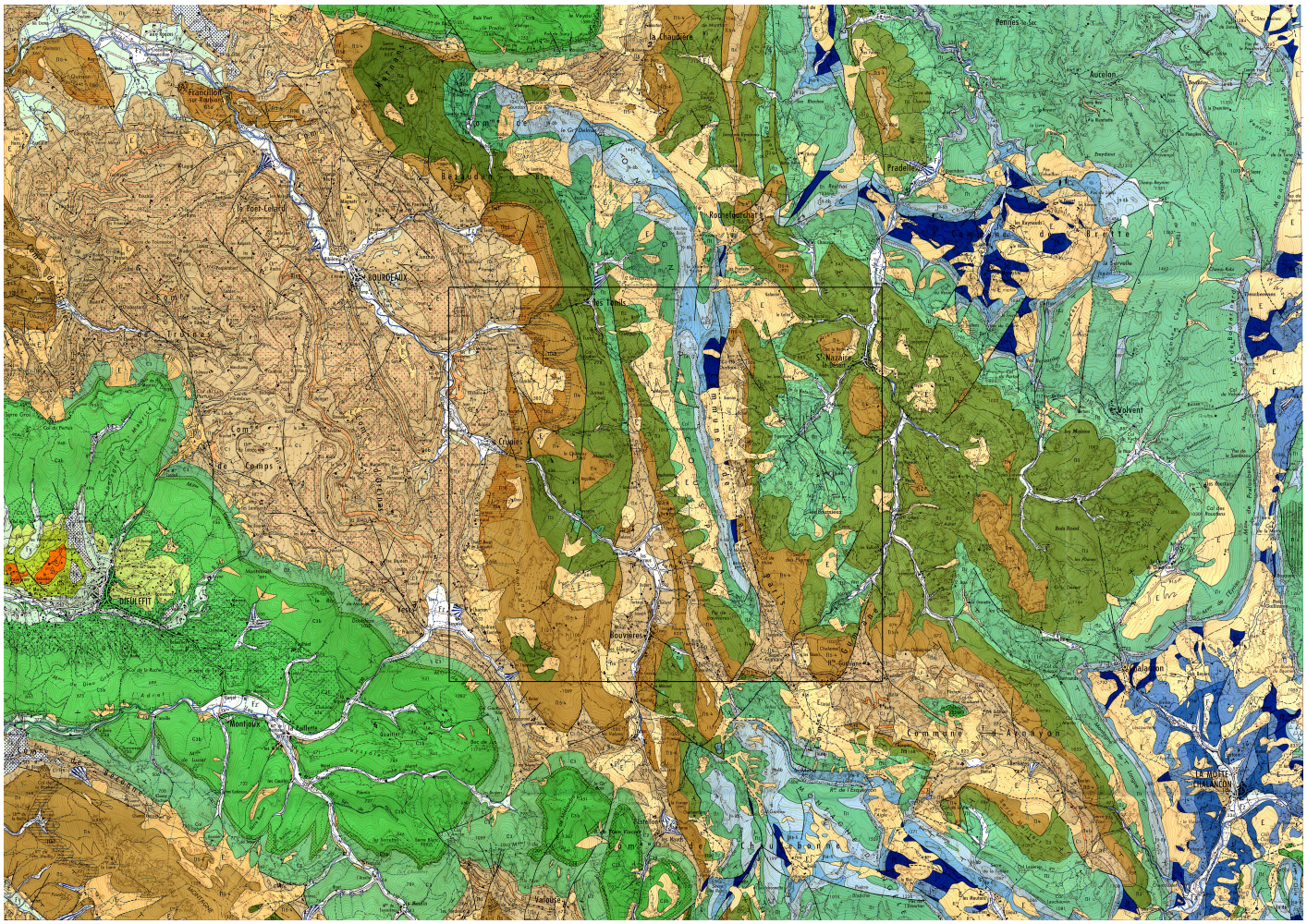

Figure 4.4: Dieulefit geologic map with the clipped area of interest

4.3 Cross sections

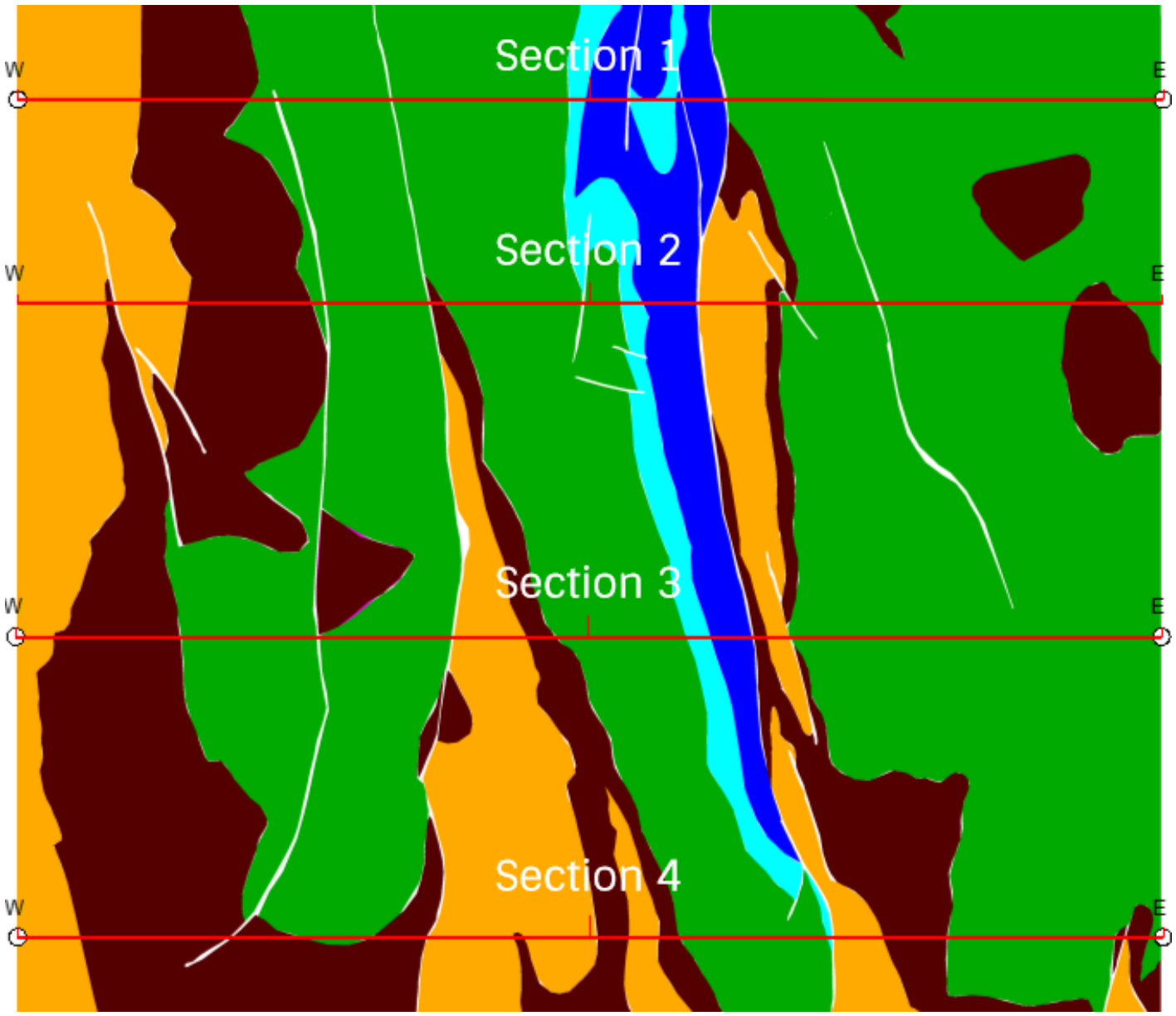

Figure 4.5: Section location map

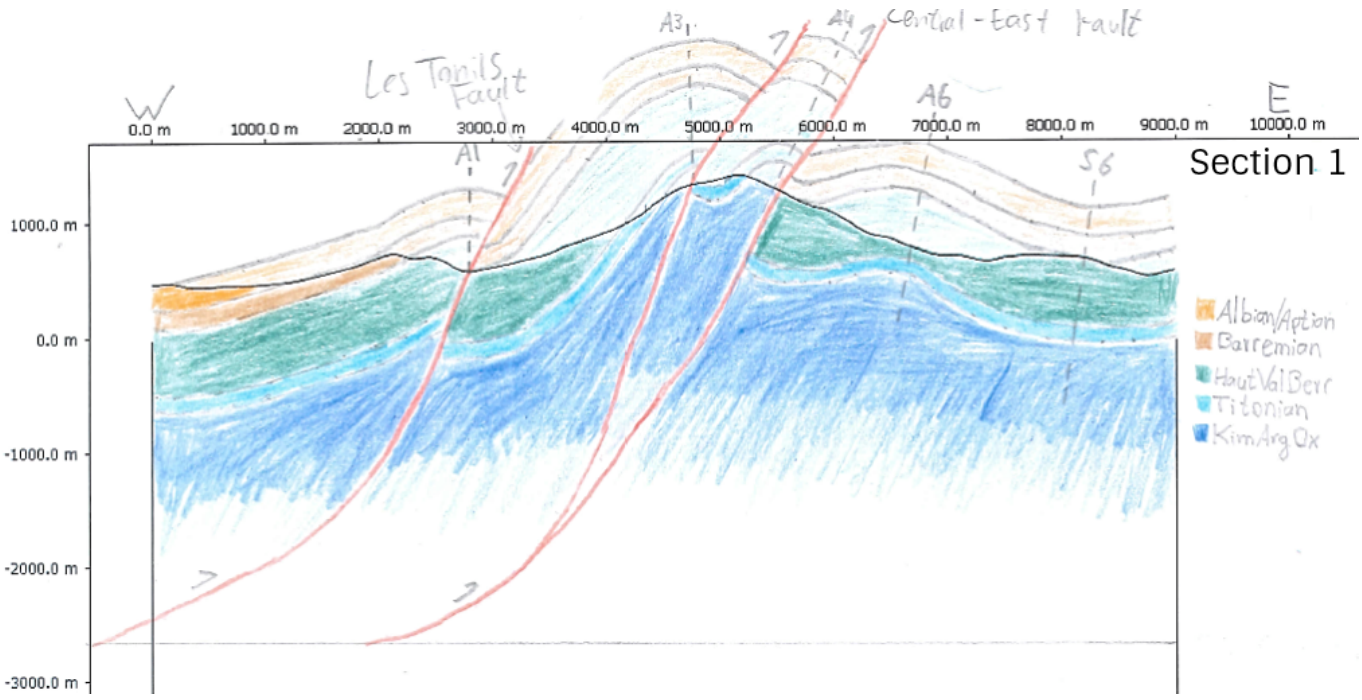

Figure 4.6: Cross section 1

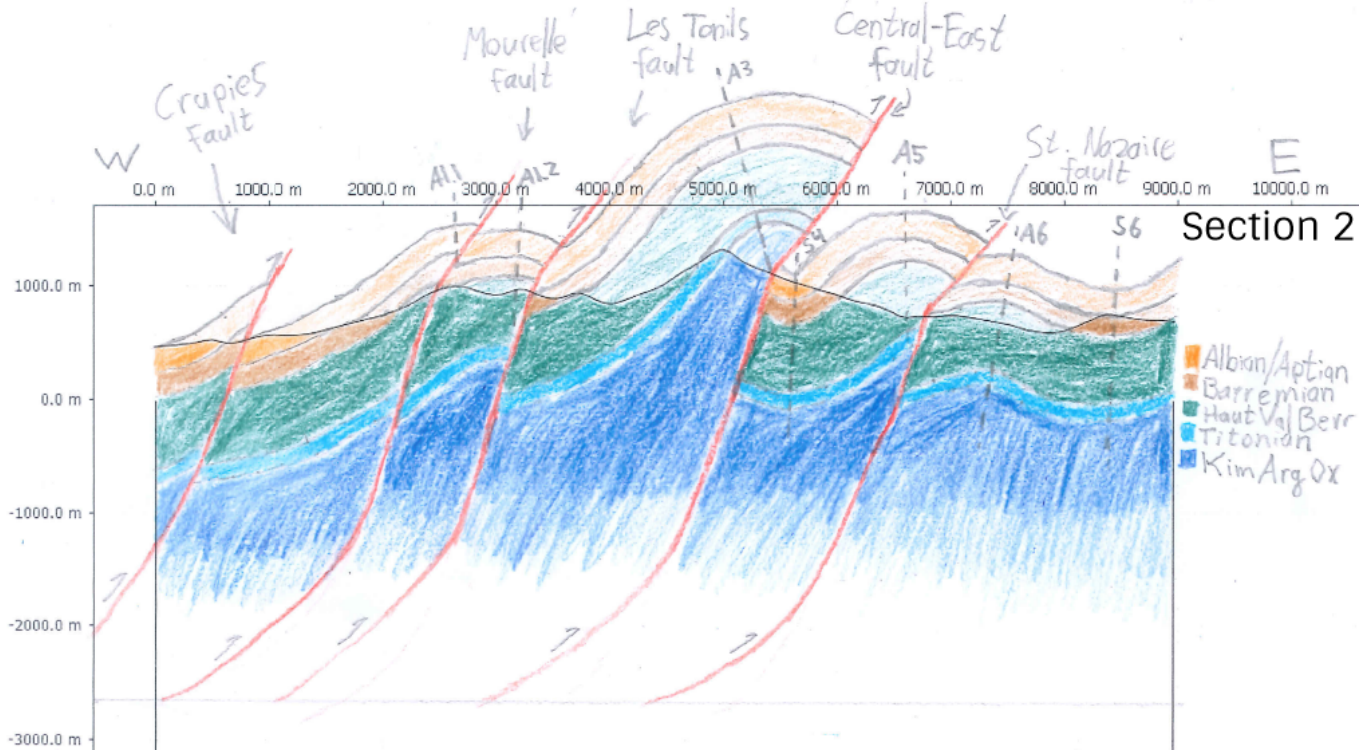

Figure 4.7: Cross section 2

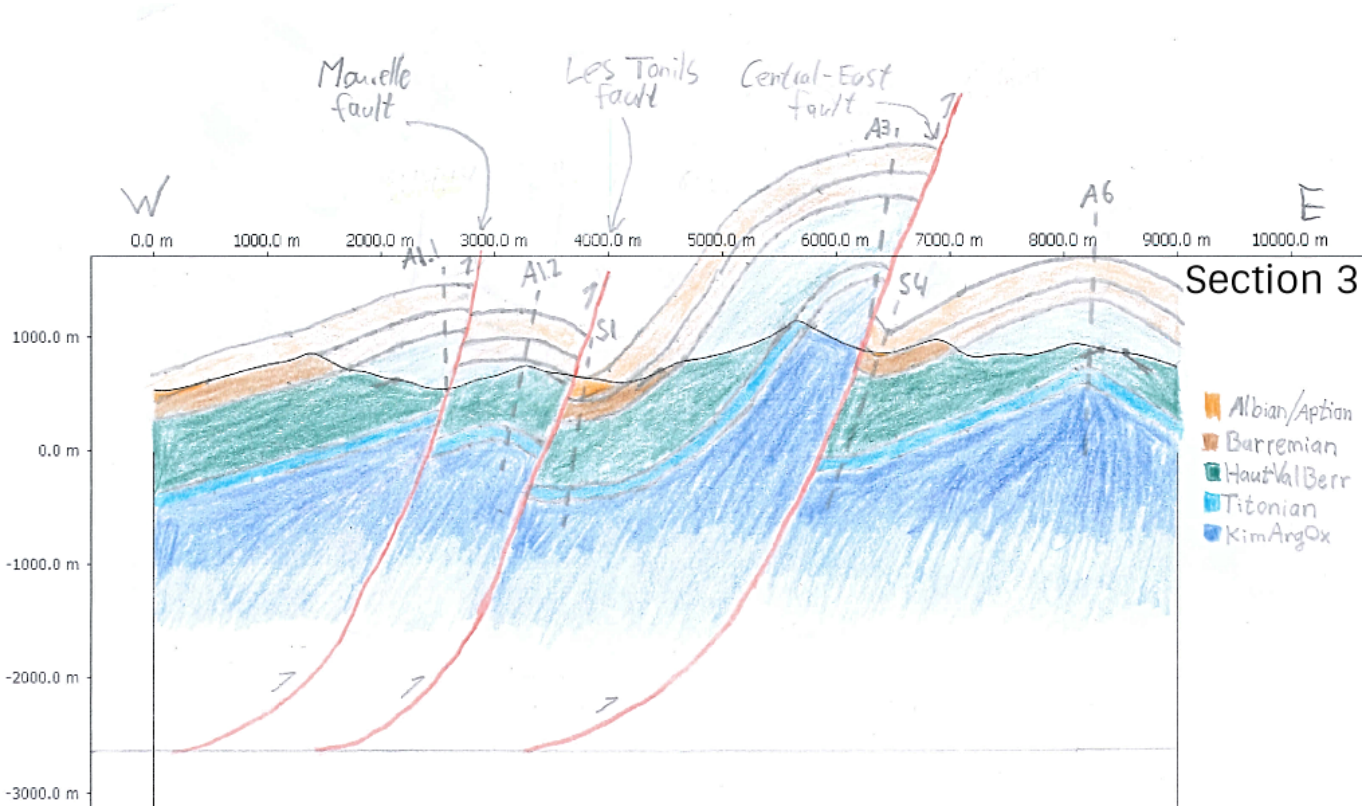

Figure 4.8: Cross section 3

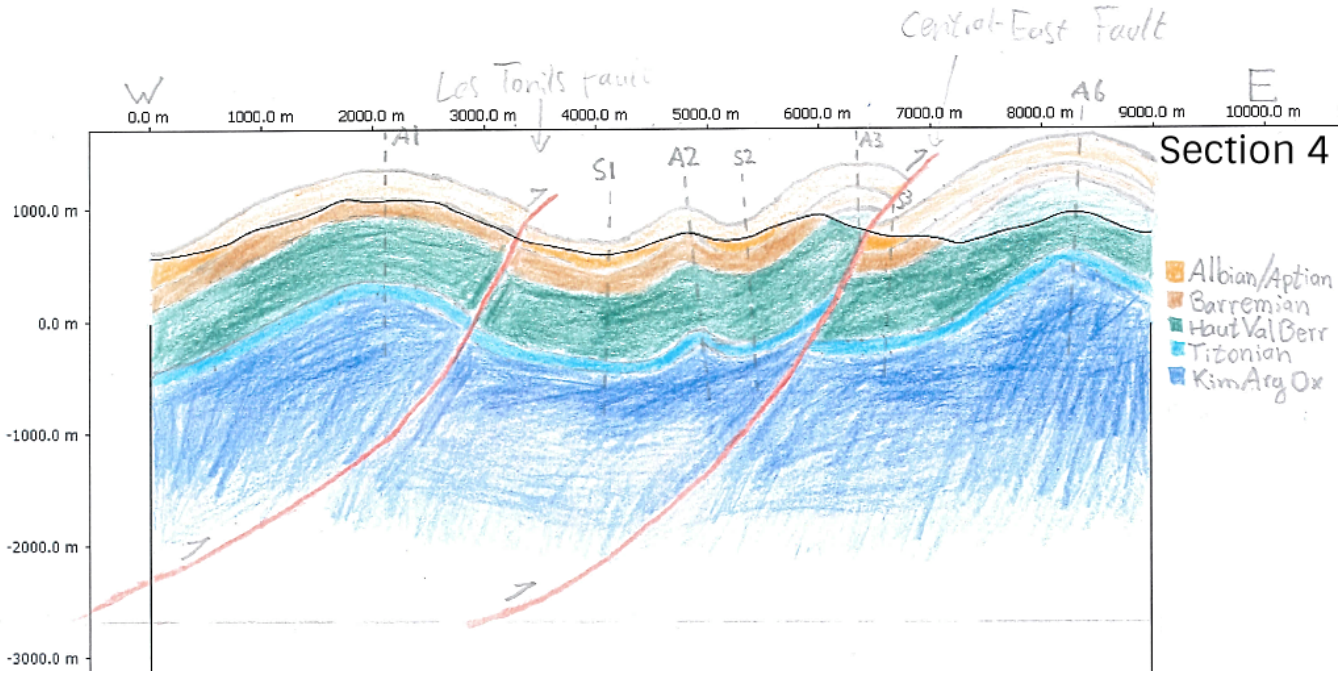

Figure 4.9: Cross section 4

5 2D modelling with Move

5.1 Digitizing the sections

All four cross sections were digitized in MOVE. To do this, first the sketched cross sections were inserted at the predetermined locations in the MOVE model. Then, the drawn sections were fitted to match the dimensions of the section in MOVE. A stratigraphic column was created such that the software could distinguish between different horizons (Figure 5.2). Then, the fault and horizon lines from the sketch were traced with the Create Lines module. An example result is shown in Figure 5.1.

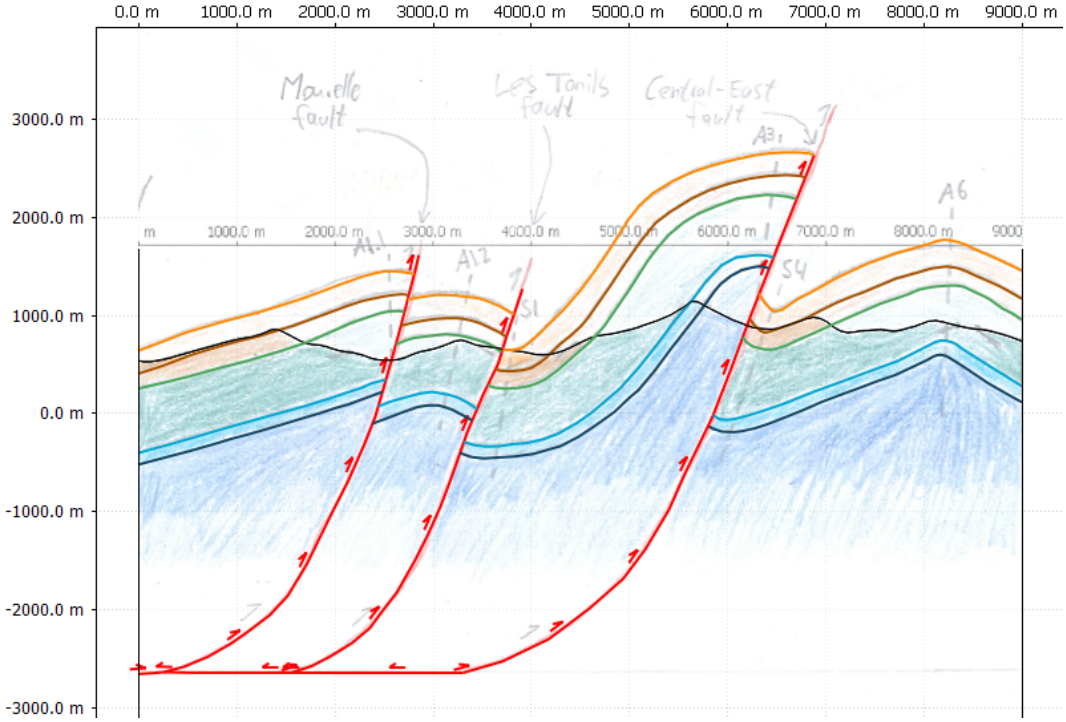

Figure 5.1: Digitized cross section by tracing the fault and horizon lines from the sketched section

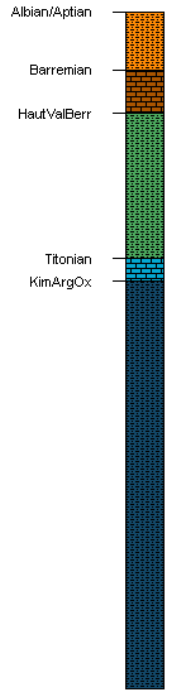

Figure 5.2: Digitized stratigraphic column

5.2 Section restoration

Section restoration has a couple of applications. One of them is to find out whether a cross section is balanced. This is done by restoring displacement along faults and unfolding the horizons in each section to a horizontal state. A 'balanced' cross section is a section which after restoration shows horizons of the same length.Bedding thicknesses remain constant during restoration. A section is defined as 'unbalanced' if these conditions are not met. In this case, revisions of the section are needed until the section can be properly restored. It should be noted that a balanced section is not necessarily correct. It simply provides a defensible and geologically feasible image of the subsurface (Nelson, Patton, & Serra, 1999).

A second application is the possibility of performing forward modelling on restored sections to discover what kind of structural mechanisms were possibly active in the area. subsection 5.3 elaborates more on 2D forward modelling.

Lastly, a restored section can be used to calculate the total amount of shortening in the area. subsection 6.3 describes how this calculation is performed.

5.2.1 Fault restoration

For this part it was assumed that faulting happened entirely after folding. This assumption was necessary to systematically, step wise perform section restoration. The first step is therefore fault restoration. During this thesis the 2D Move-on-Fault module in MOVE was used. Within this module, the Fault Parallel Flow algorithm was selected to perform the restoration. This algorithm works by marking changes in the fault's dip by dip bisectors. These dip bisectors are used to construct flow lines along which the horizons in the hanging wall can be translated (Petroleum Experts Ltd., 2019). The distance of translation is defined by manually choosing a horizon in the hanging wall and foot wall from the same formation, and let these beds join. All horizons are displaced the same distance as the joined beds. This way the bedding thicknesses remain constant (Petroleum Experts Ltd., 2019).

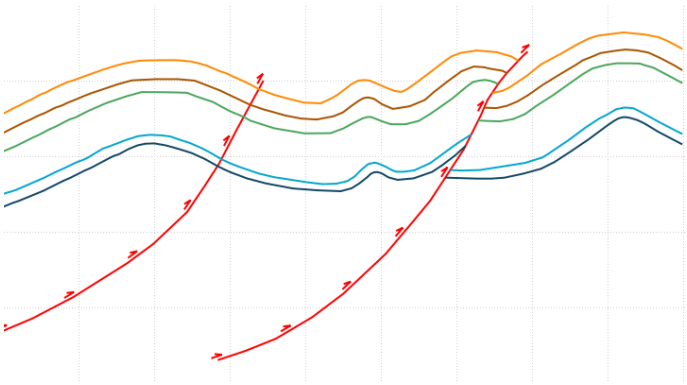

Figure 5.3: Section before translation

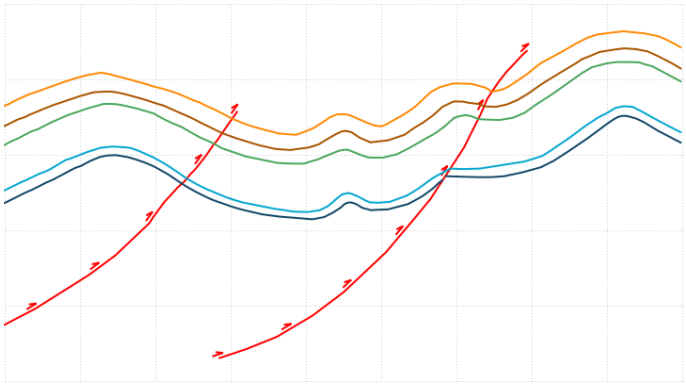

Figure 5.4: Section after translation along fault

Sometimes after fault restoration, small horizon discontinuities at the active fault surface occur. This is due to minor mistakes made during sketching and/or digitizing. If the discontinuities are too major, the section is flawed and needs revision. In case of a minor discontinuity, like shown in Figure 5.5b, the horizon lines can be manually edited to fix the problem.

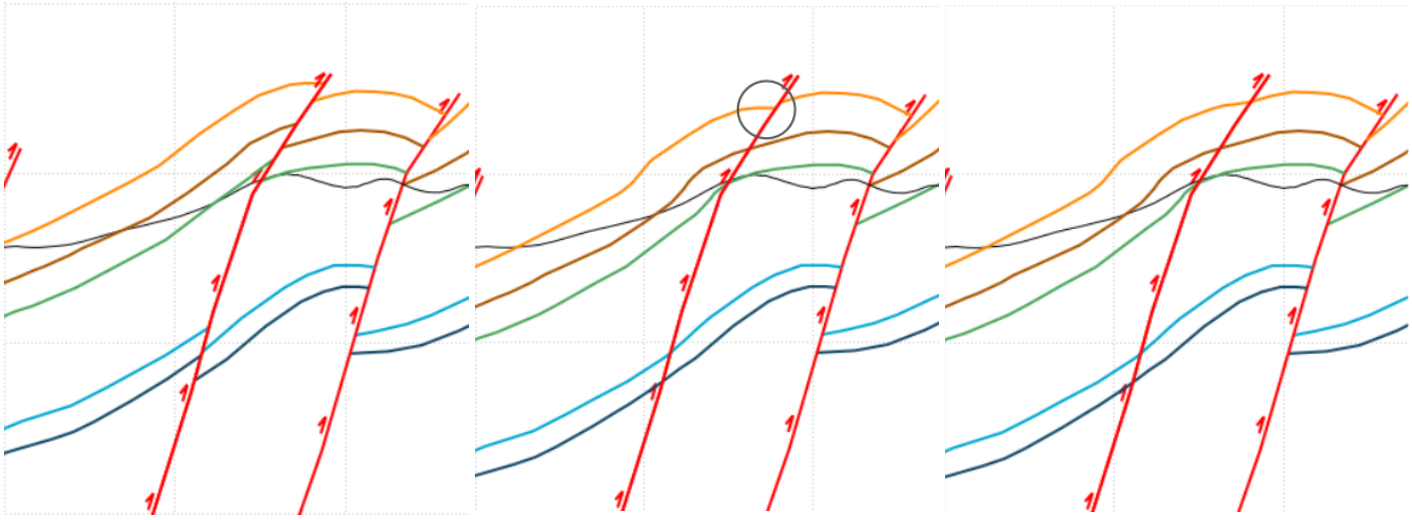

(a) Before restoration

(b) After fault restoration

(c) Adjusted horizon discontinuity

Figure 5.5

5.2.2 Unfolding

The 2D Unfolding module in MOVE was used to unfold the sections after fault restoration. Within this module, the Flexural Slip Unfolding algorithm was selected. The algorithm works by rotating the limbs of a fold to a datum (Petroleum Experts Ltd., 2019). This datum is a manually chosen template horizon, the other horizons are passive horizons. Subsequently, the algorithm applies layer parallel shear to remove the effects of flexural slip. A pin has to be manually set which should correspond to the axial surface of a fold (Petroleum Experts Ltd., 2019). The pin marks the surface of no slip. Figure 5.6 shows the location of the pin before flexural unfolding.

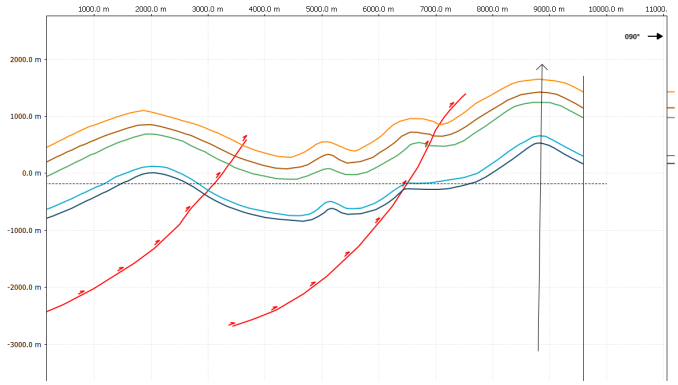

Figure 5.6: Set-up before Flexural Slip Unfolding

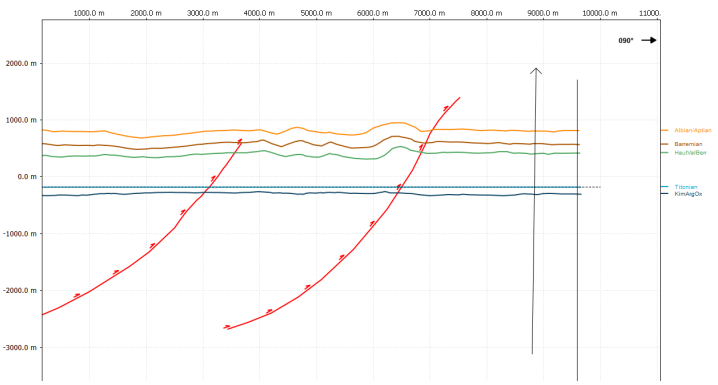

Figure 5.7: A Flexural Slip Unfolded section.

After Flexural Slip Unfolding, minor increments remain in the passive horizons (Figure 5.7). The Line Length Unfolding algorithm can be used to flatten these remaining bumps. This algorithm works by rotating the limbs of a fold to a undeformed state represented by a perfect straight line (Petroleum Experts Ltd., 2019). The line length is preserved, however the bedding thickness is often not preserved. That's why this algorithm should not be used before Flexural Slip Unfolding, but rather only to restore remaining minor increments.

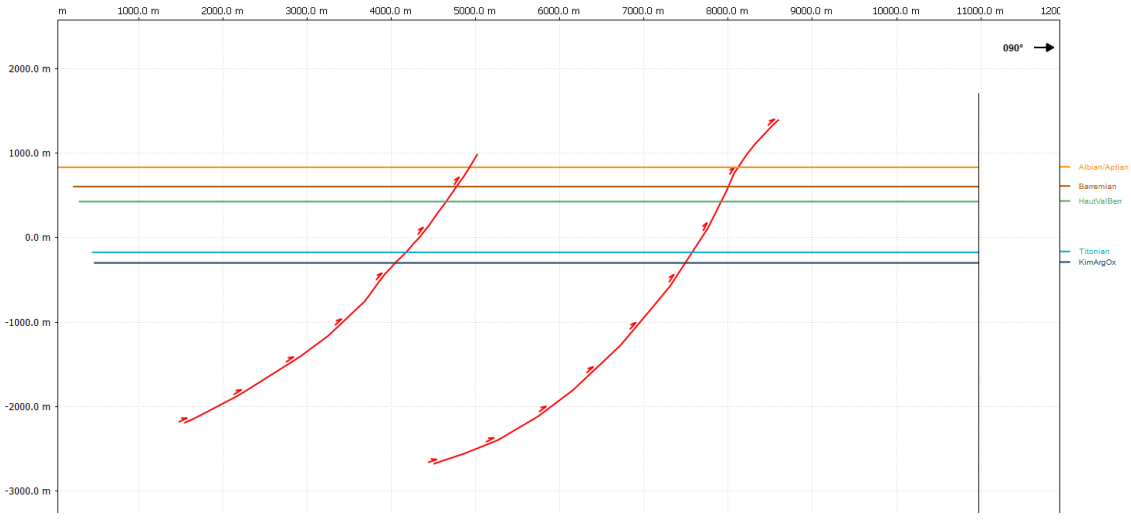

Figure 5.8: Restored section after Flexural Slip and Line Length unfolding

Figure 5.8 shows section 03 after restoration. It can be observed that bedding thicknesses remained the same. Notice that the line lengths differ from top to bottom. This is to be expected due to the fact that this area contains many anticlines, and lines at the top of an anticline are longer than those at the bottom. This section can therefore be labelled as balanced.

5.3 2D Forward modelling

One of the goals of 2D forward modelling is to check what kind of mechanisms can explain the present-day deformation. Forward modelling starts out with a restored, balanced section like the one shown in Figure 5.8. The 2D Move-on-Fault module is used again. Within the module a couple of possible thrusting mechanisms can be selected. By making use of trial and error forward modelling, a feasible thrusting mechanism could be chosen which created the best resemblance of the original cross section. Possible mechanisms include fault-propagation folding, fault-bend folding and fault parallel flow. Each of these methods create different types of folds (Watkins et al., 2015). The method which resulted in the most accurate models was the Fault-Bend Fold algorithm. This algorithm works by developing a response to a vertical step in the detachment level of the fault. It is assumed that folding is parallel to the fault and is therefore controlled by the fault surface geometry (Petroleum Experts Ltd., 2019). The amount of displacement along the fault surface can be manually adjusted until the model resembles the original interpretation.

Next to the 2D Move-on-Fault module, the 2D Unfolding module could also be used for forward modelling. The Flexural Slip algorithm can fold horizons to a specific datum. If this datum exactly corresponds to the original folded horizon, then the result is an accurate resemblance of the present-day situation. This method was applied in situations where it was assumed that not faulting, but folding was the main reason for deformation.

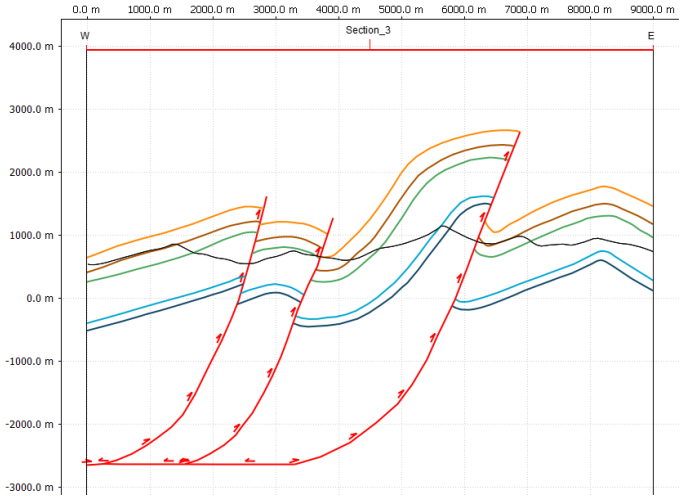

Figure 5.9: Original interpreted section

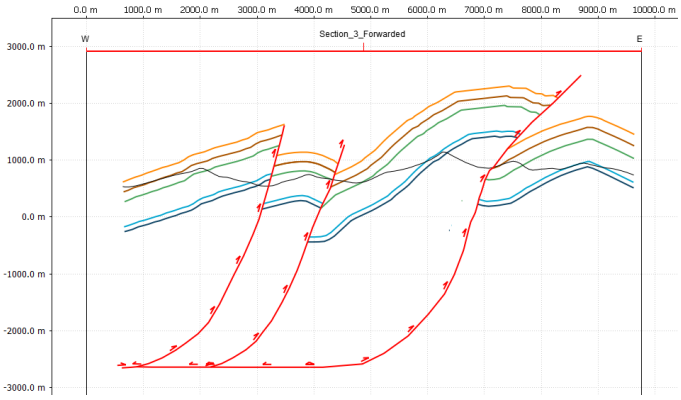

Figure 5.10: Forward modelled section using Fault-bend Folding and Flexural Unfolding

Notice when looking at Figure 5.9 and Figure 5.10 that although the forwarded model does resemble the original interpretation, they aren't exactly the same. The large thrust fault on the right side of the images has been adjusted to a more horizontal geometry towards the top, so that the Fault-bend Fold algorithm could create a better result. Forward modelling is an iterative process during which minor adjustments of the original interpretation will be necessary. This can result in the discovery that the original interpretation is flawed and needs revision. In the example case of Figure 5.9 this means that the large fault on the right was probably flawed in the original interpretation, and should resemble a geometry more like the one shown in Figure 5.10.

5.4 Strain modelling

Measuring strain provides the opportunity to map out strain variations caused by different structural methods. The strain data can help to understand the shear zones in an orogenic setting. Strain can also help to determine the driving mechanisms in folded and faulted zones (Fossen, 2010). During forward modelling, strain circles were included in the examined formations. The shape of the deformed circles contains information on how the deformation occurred (Fossen, 2010). Circles which remain circular indicate little deformation in that location. Circles which become oblate or flattened out indicate locations of higher deformation. For this thesis only the planar strain was measured.

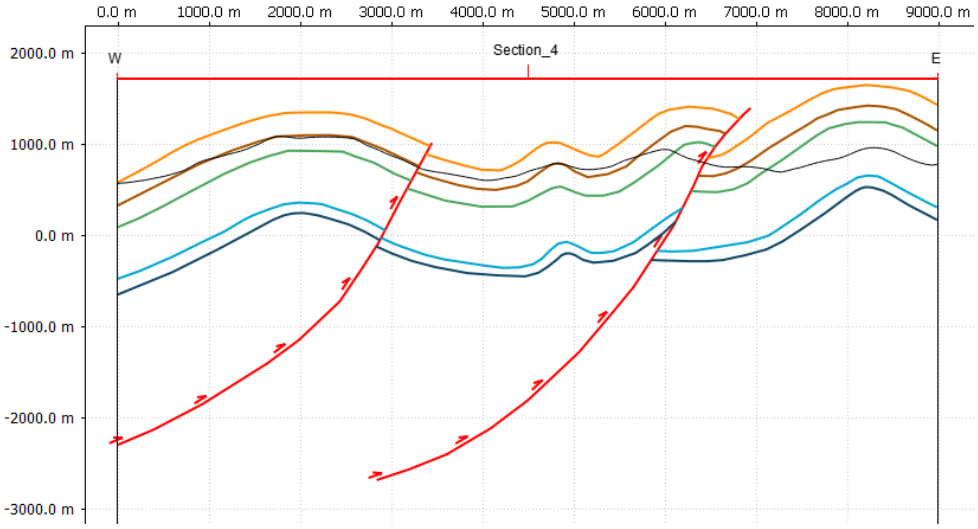

Figure 5.11: Original interpreted section

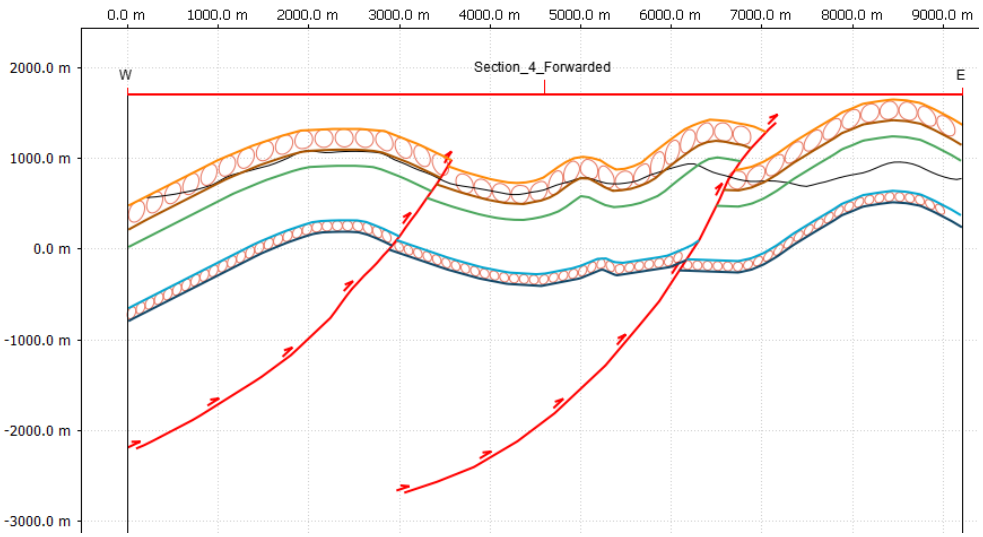

Figure 5.12: Forward model with strain circles included

6 Results

6.1 Structural map

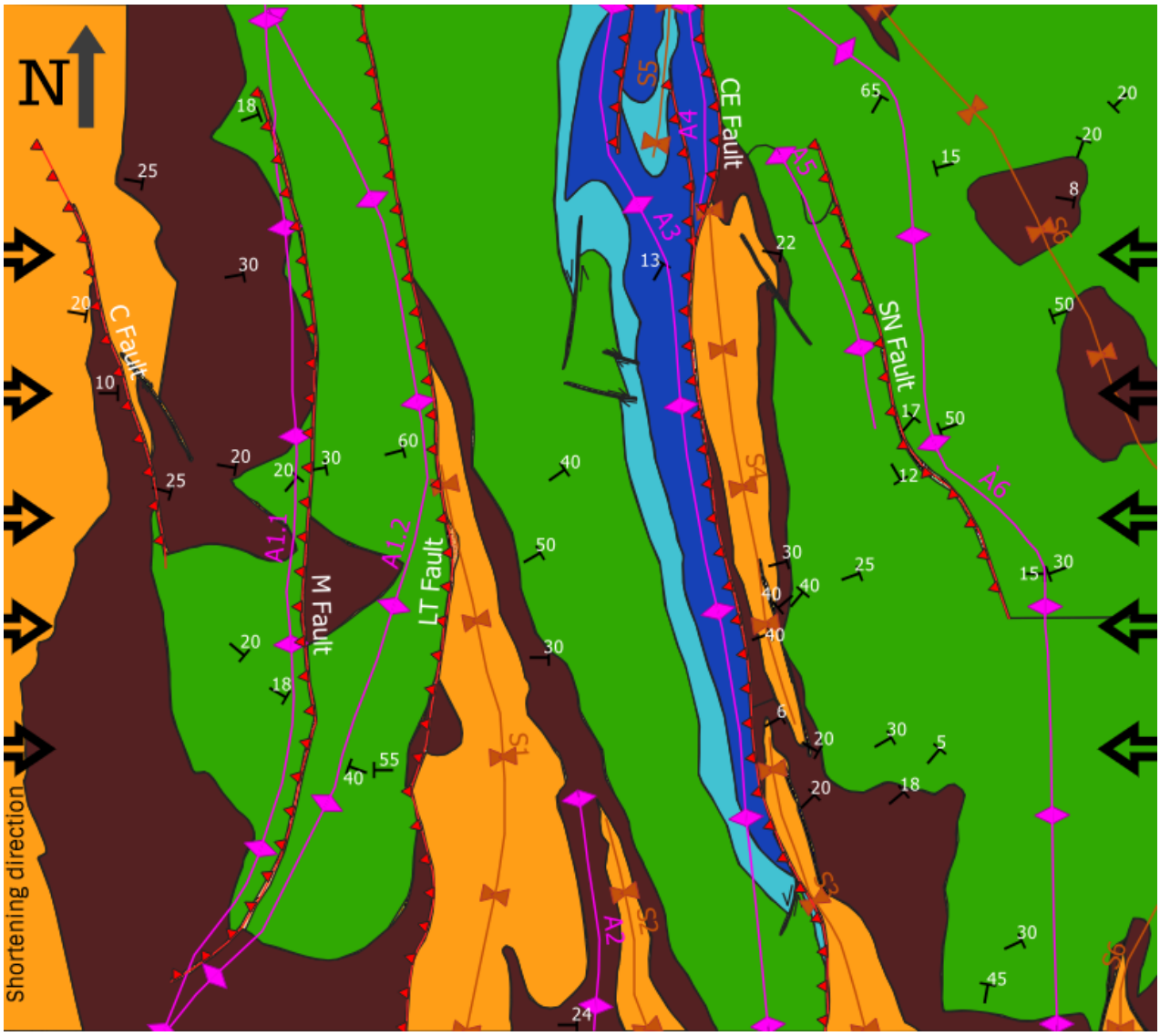

(a) Structural map of the Couspeau area

(b) Legend

Figure 6.1

6.2 Cross sections

6.2.1 Section 1

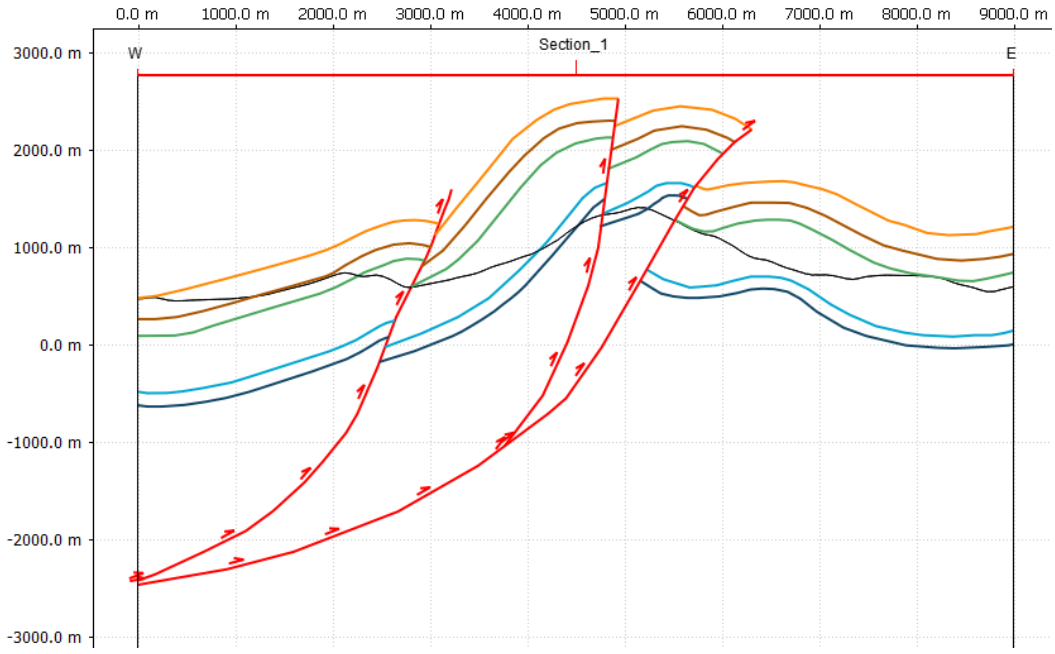

Figure 6.2: Digitized section 1

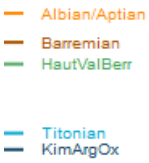

Figure 6.3: Legend for cross section horizons

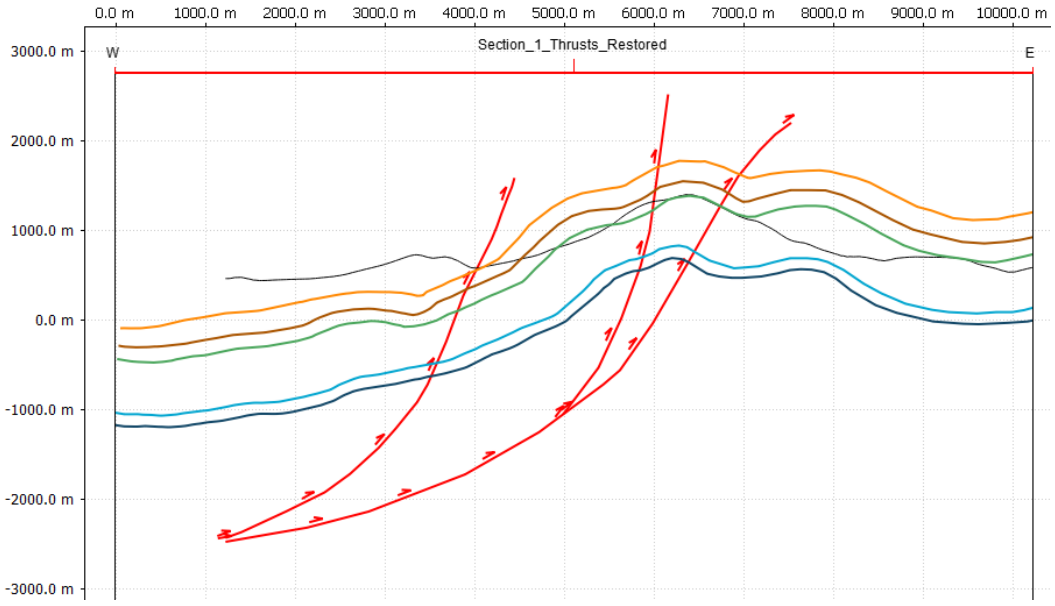

Figure 6.4: Restored fault displacement

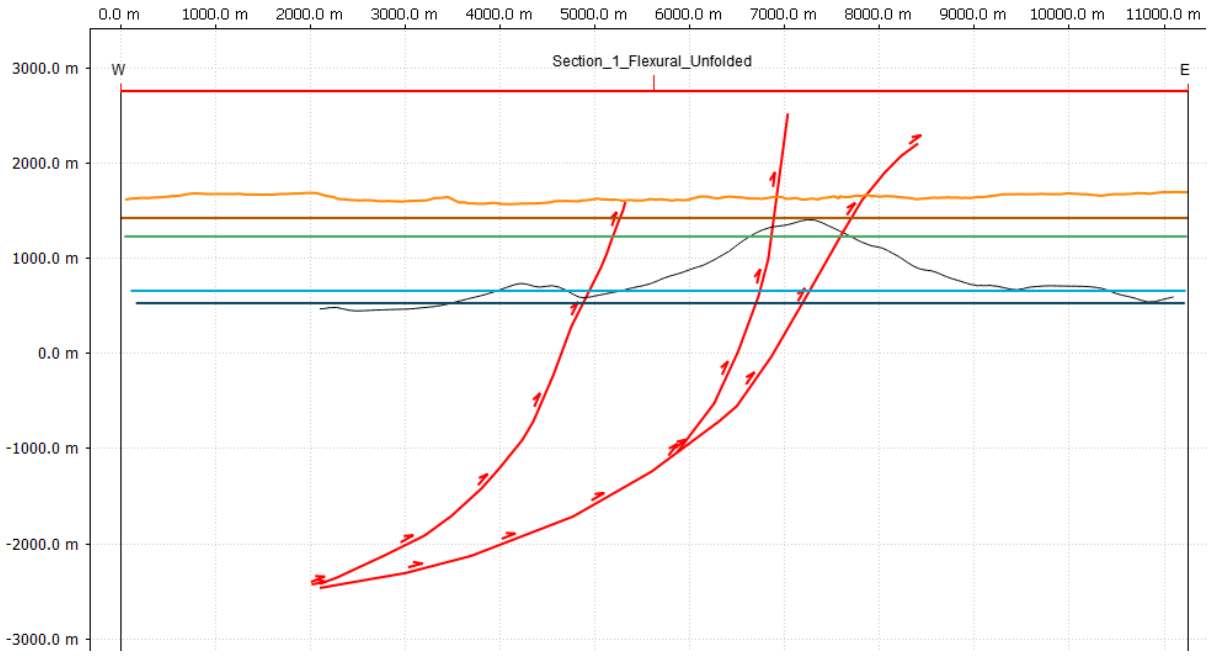

Figure 6.5: Flexural slip unfolded

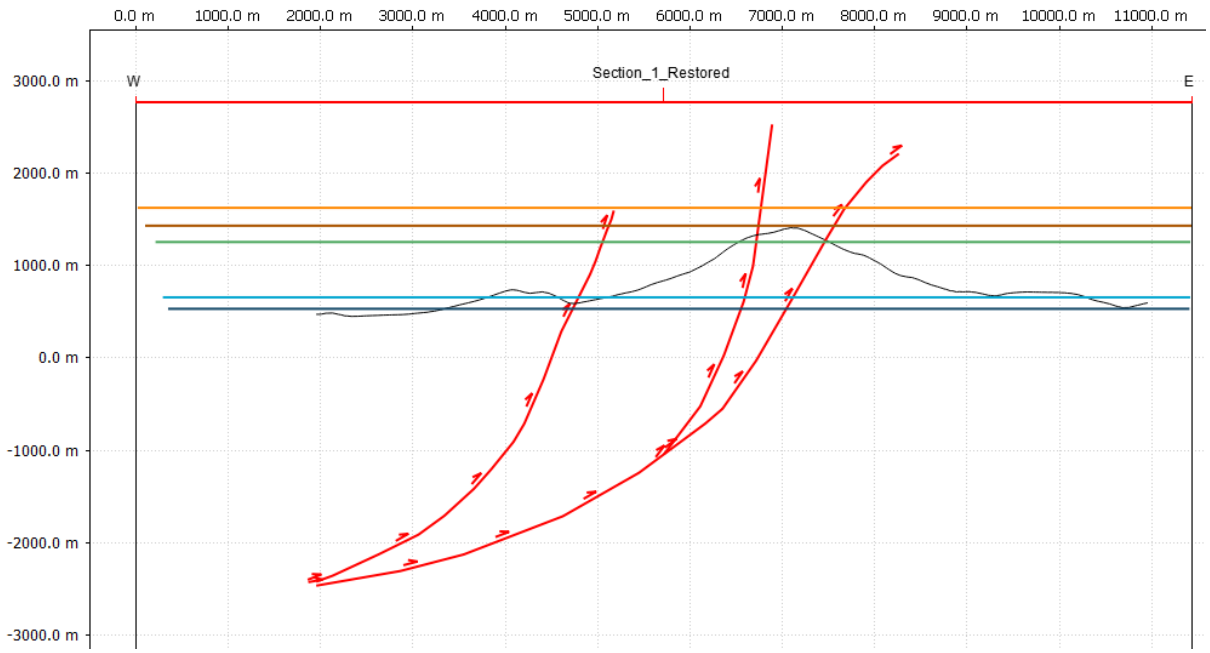

Figure 6.6: Line Length unfolded

6.2.2 Section 2

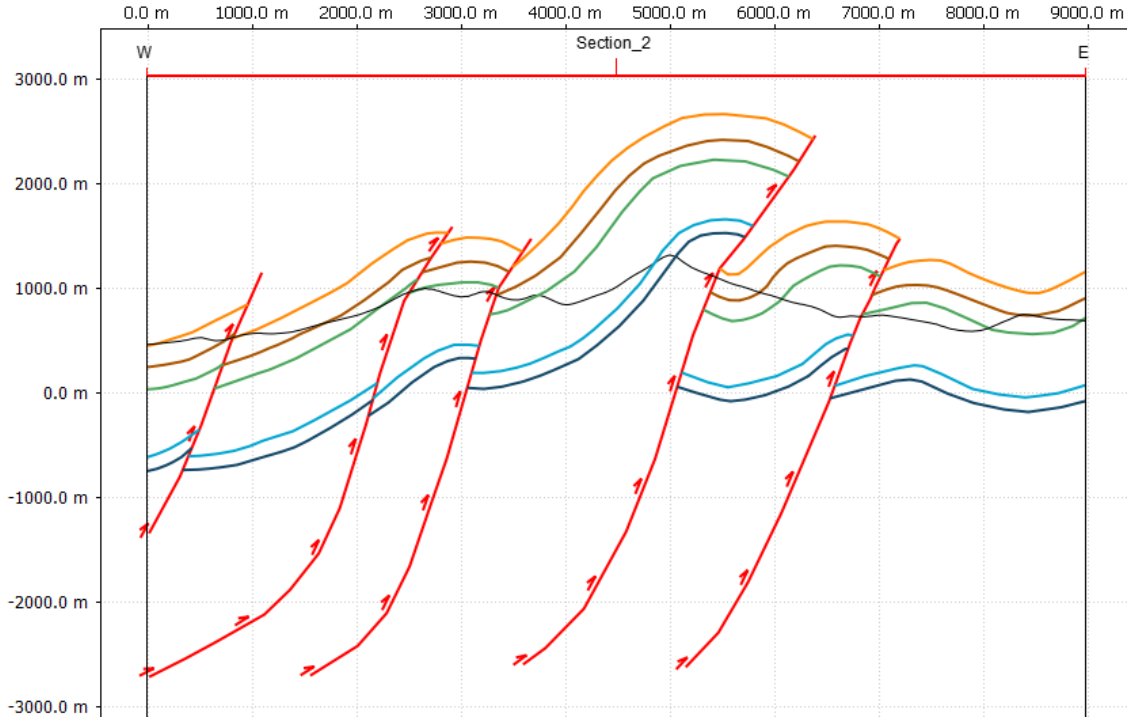

Figure 6.7: Digitized section 2

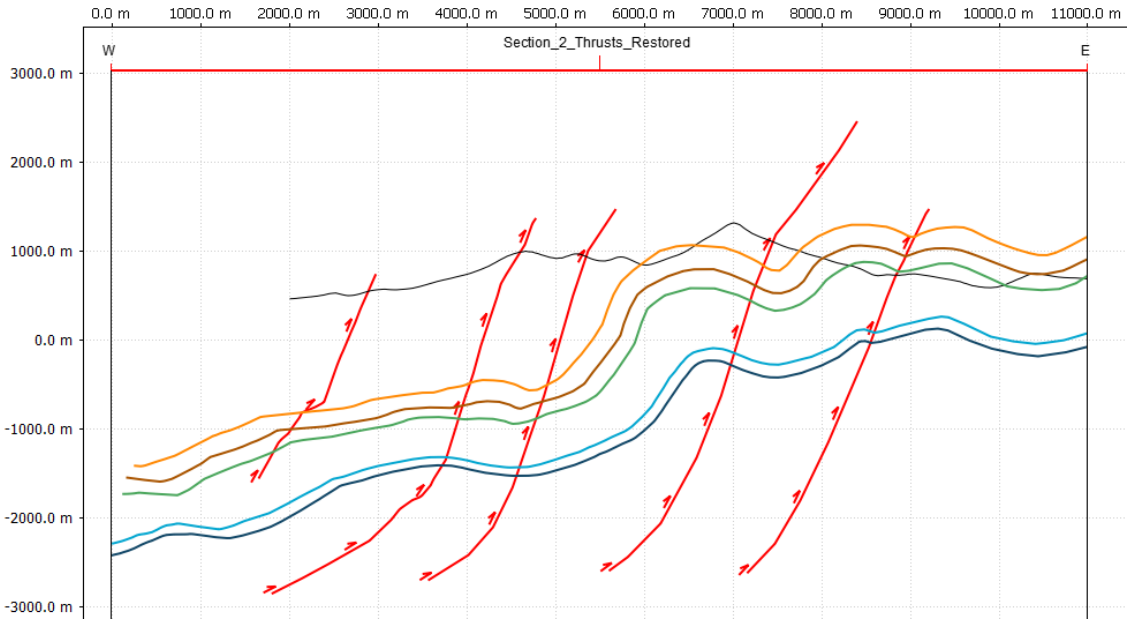

Figure 6.8: Restored fault displacement

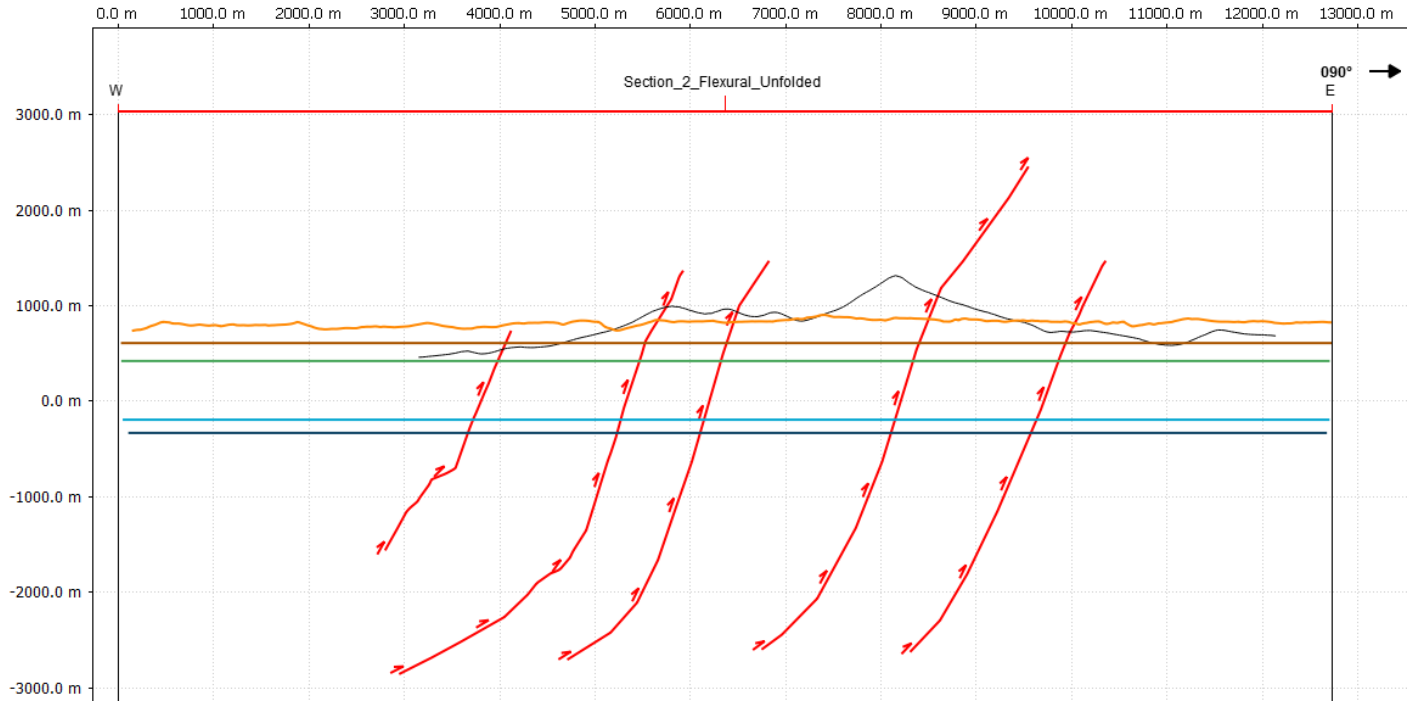

Figure 6.9: Flexural slip unfolded

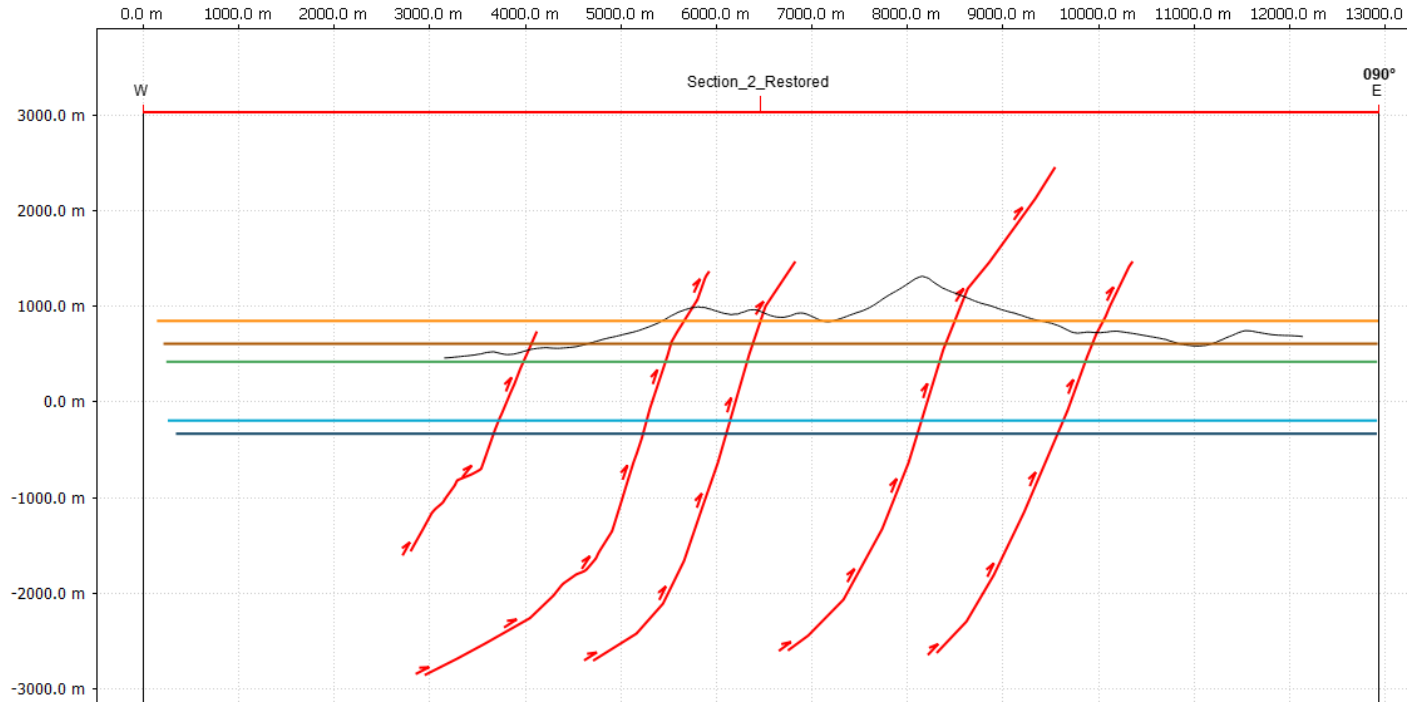

Figure 6.10: Line length unfolded

6.2.3 Section 3

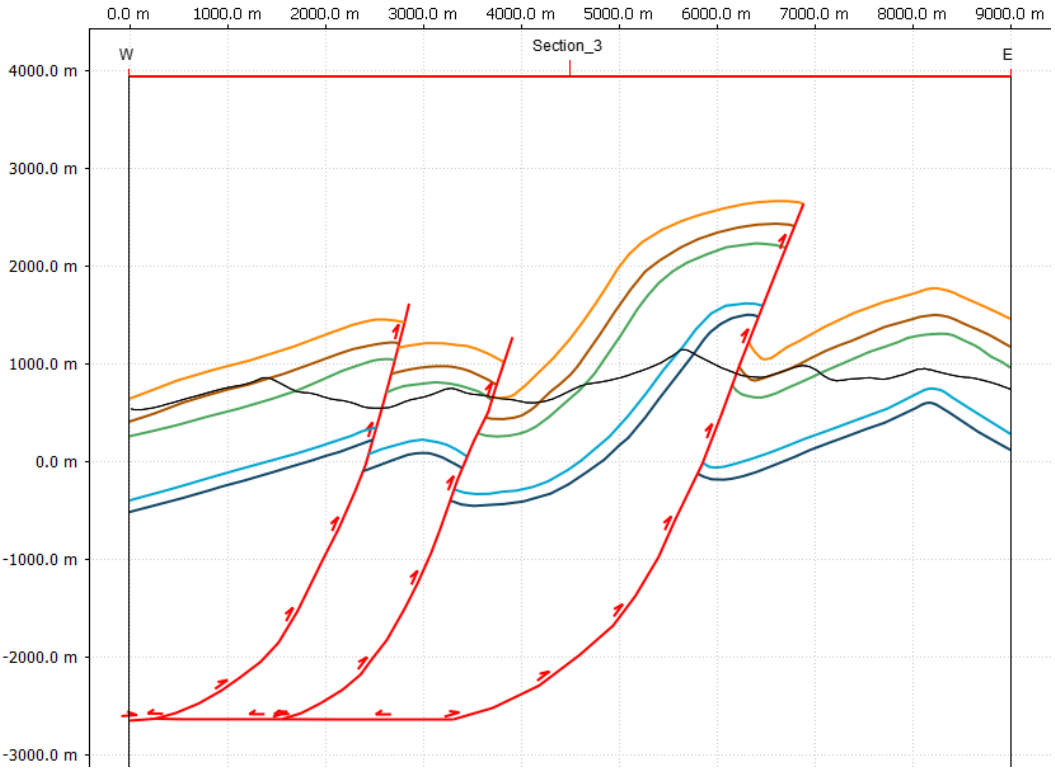

Figure 6.11: Digitized section 3

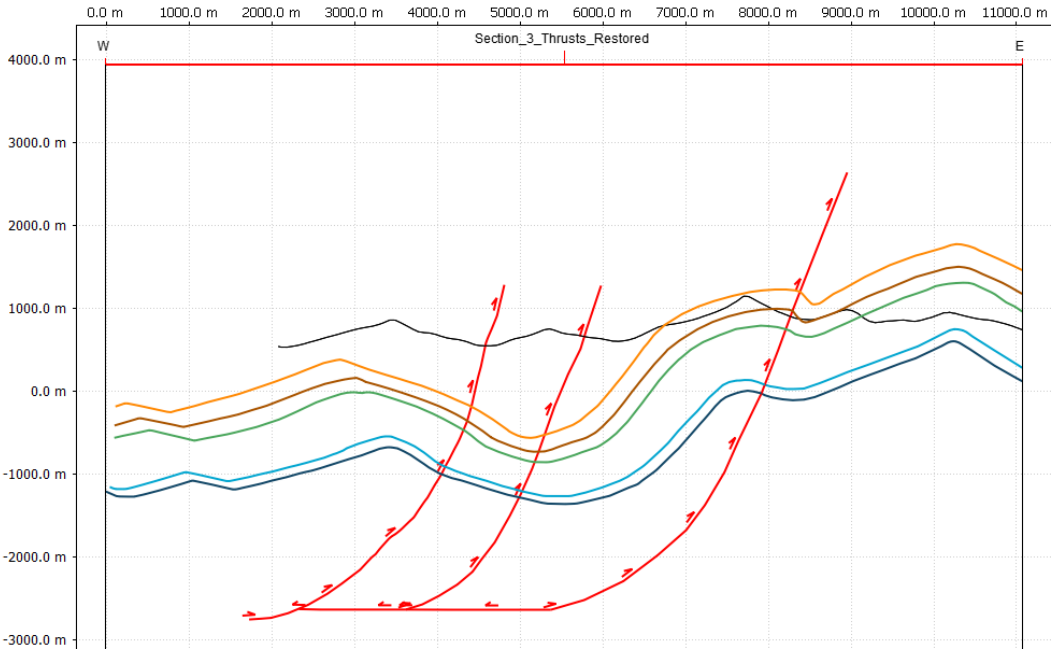

Figure 6.12: Restored fault displacement

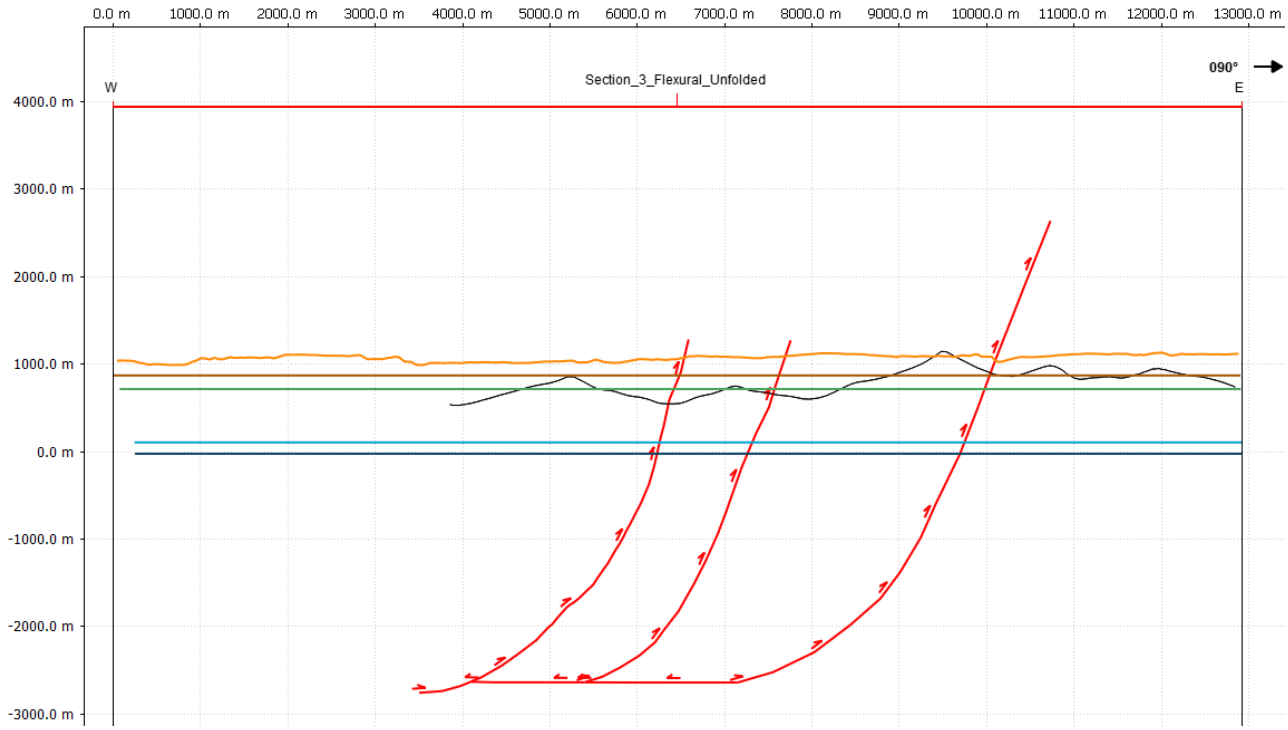

Figure 6.13: Flexural slip unfolded

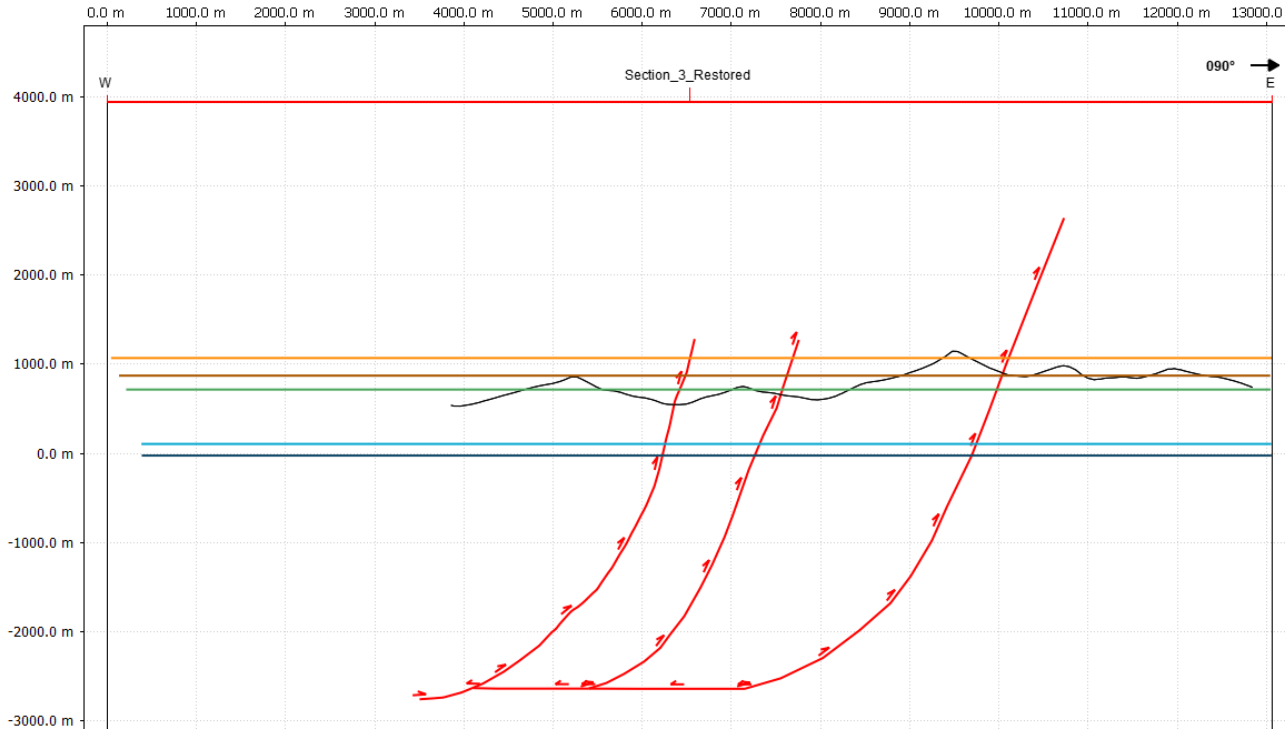

Figure 6.14: Line length unfolded

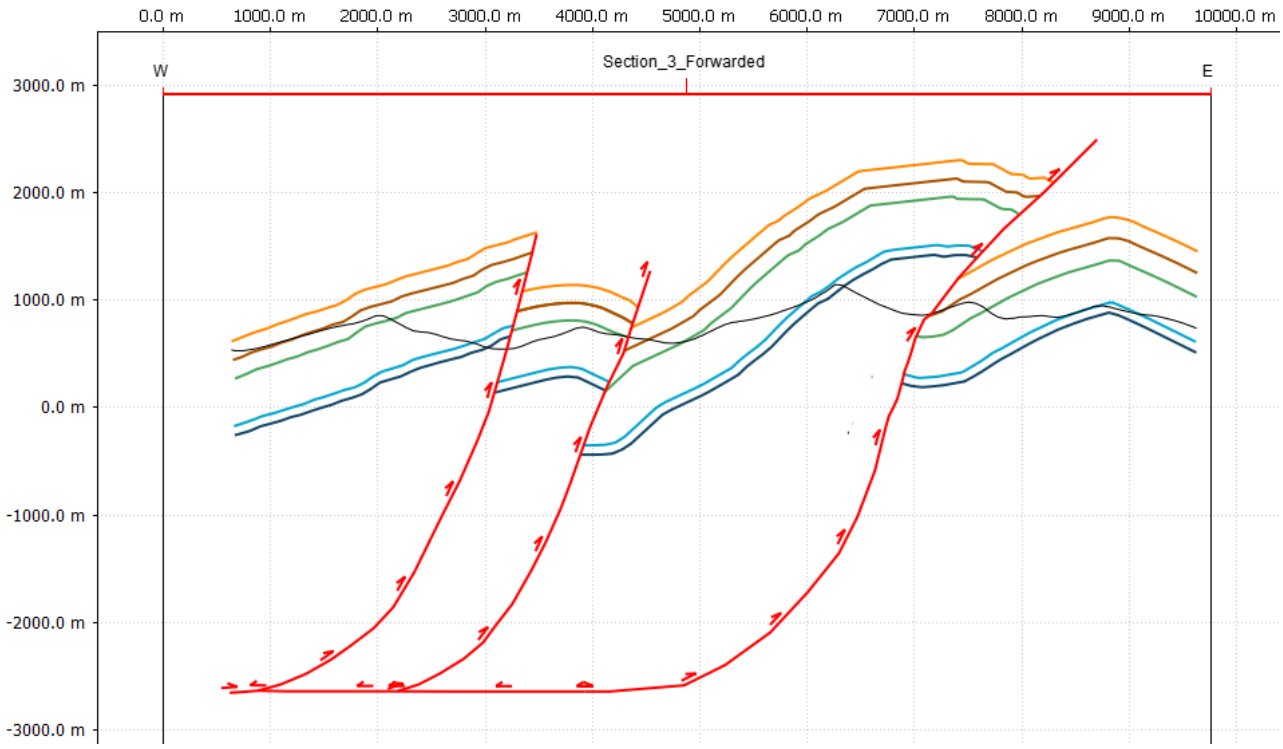

Figure 6.15: Forward model

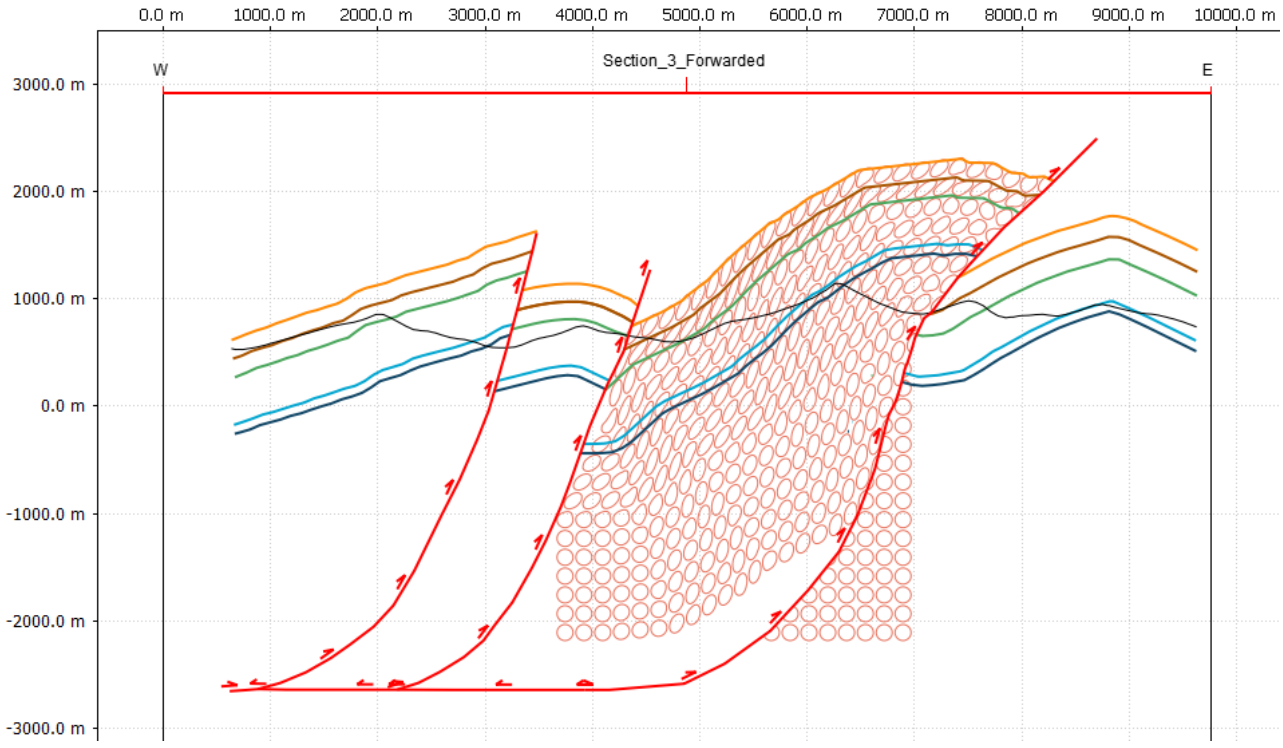

Figure 6.16: Forward model including strain circles

6.2.4 Section 4

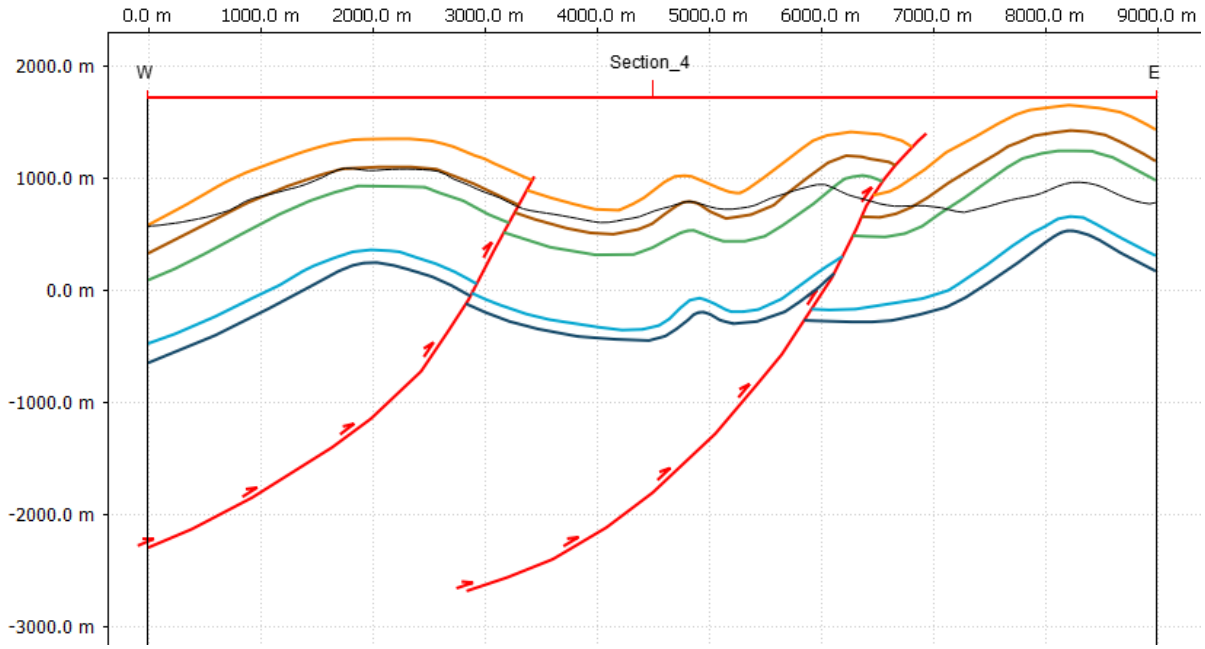

Figure 6.17: Digitized section 4

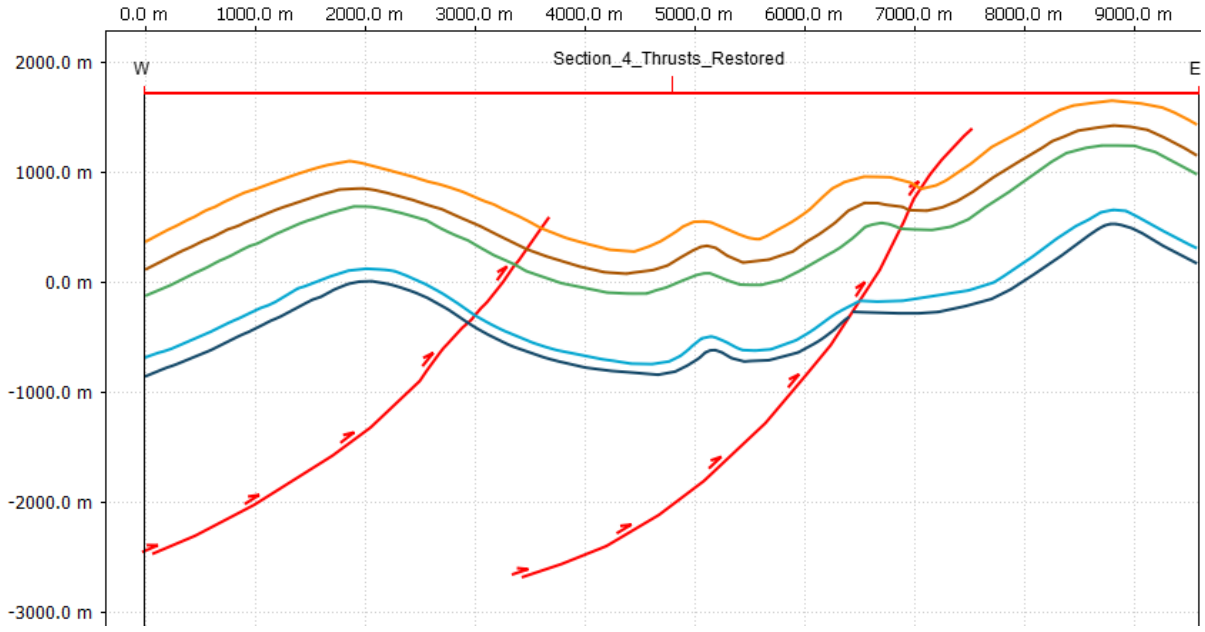

Figure 6.18: Restored fault displacement

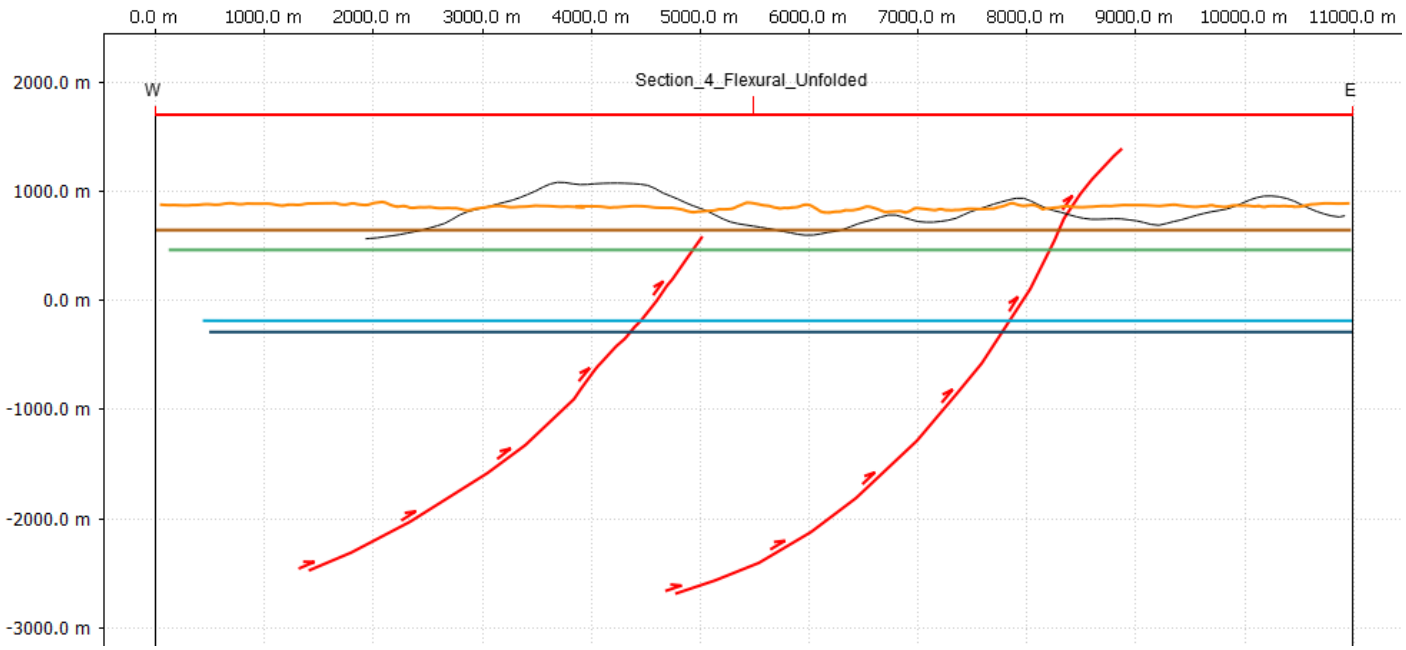

Figure 6.19: Flexural slip unfolded

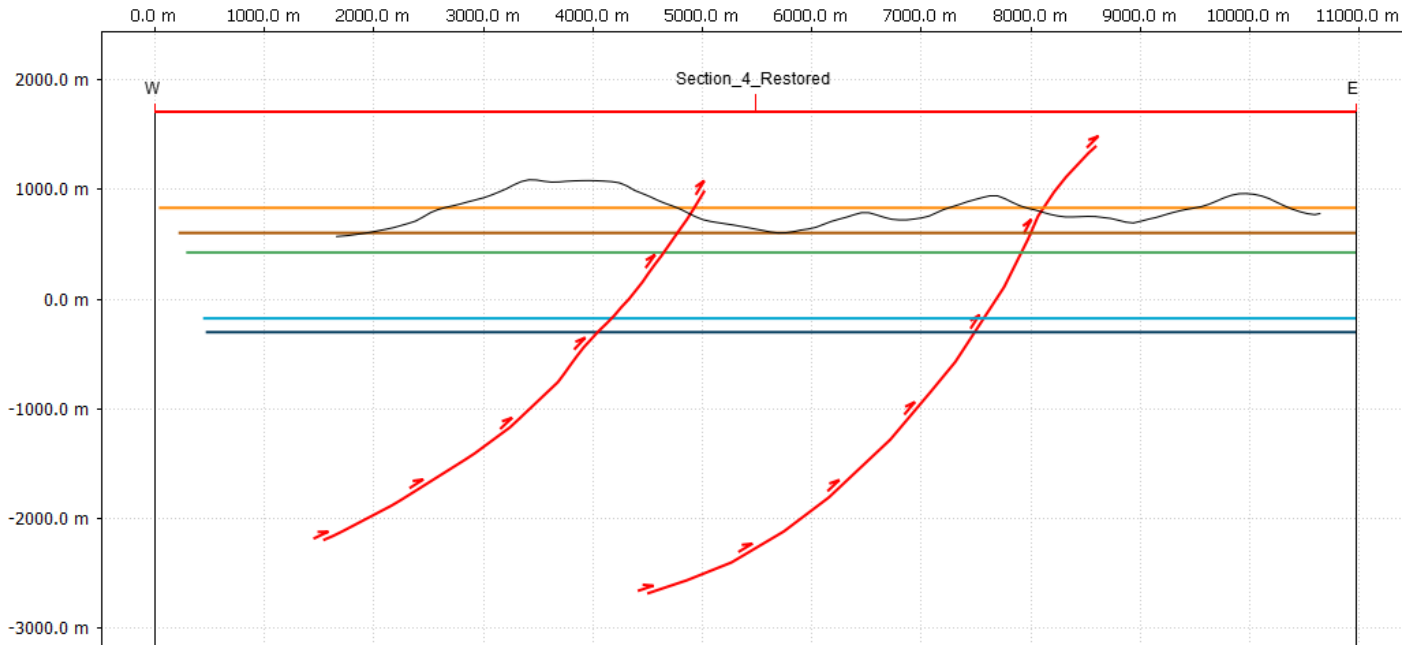

Figure 6.20: Line length unfolded

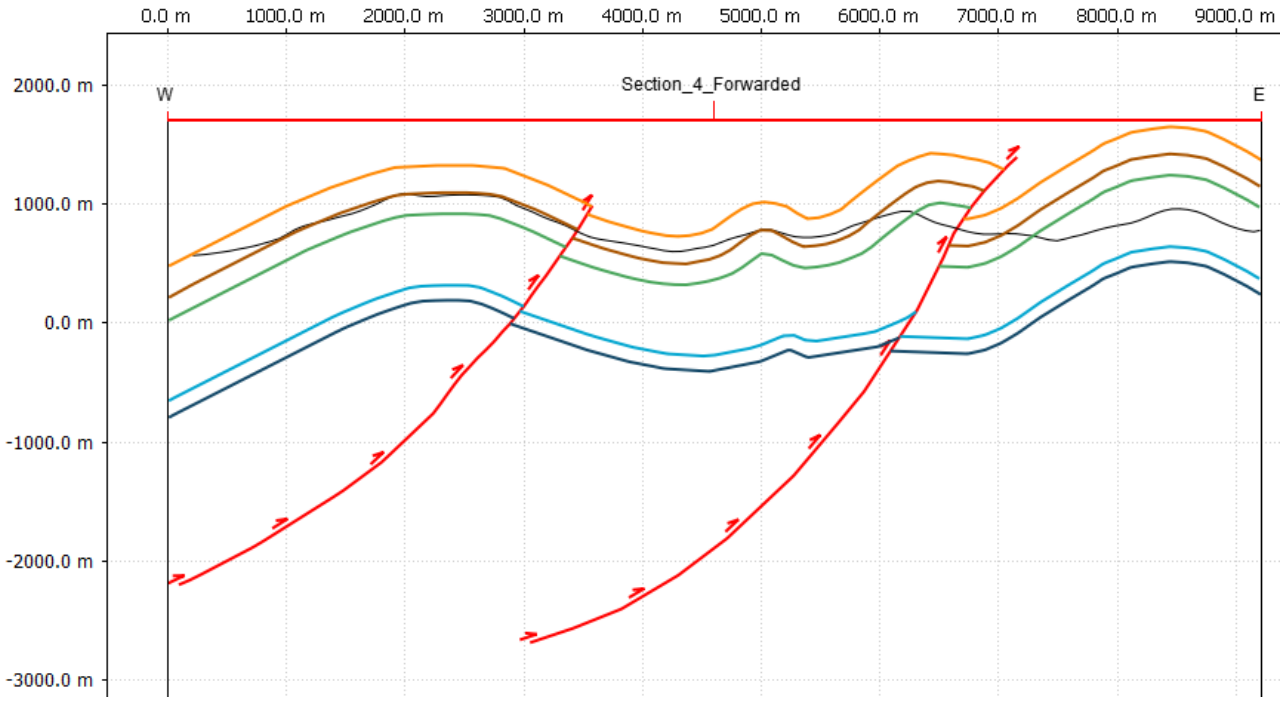

Figure 6.21: Forward model

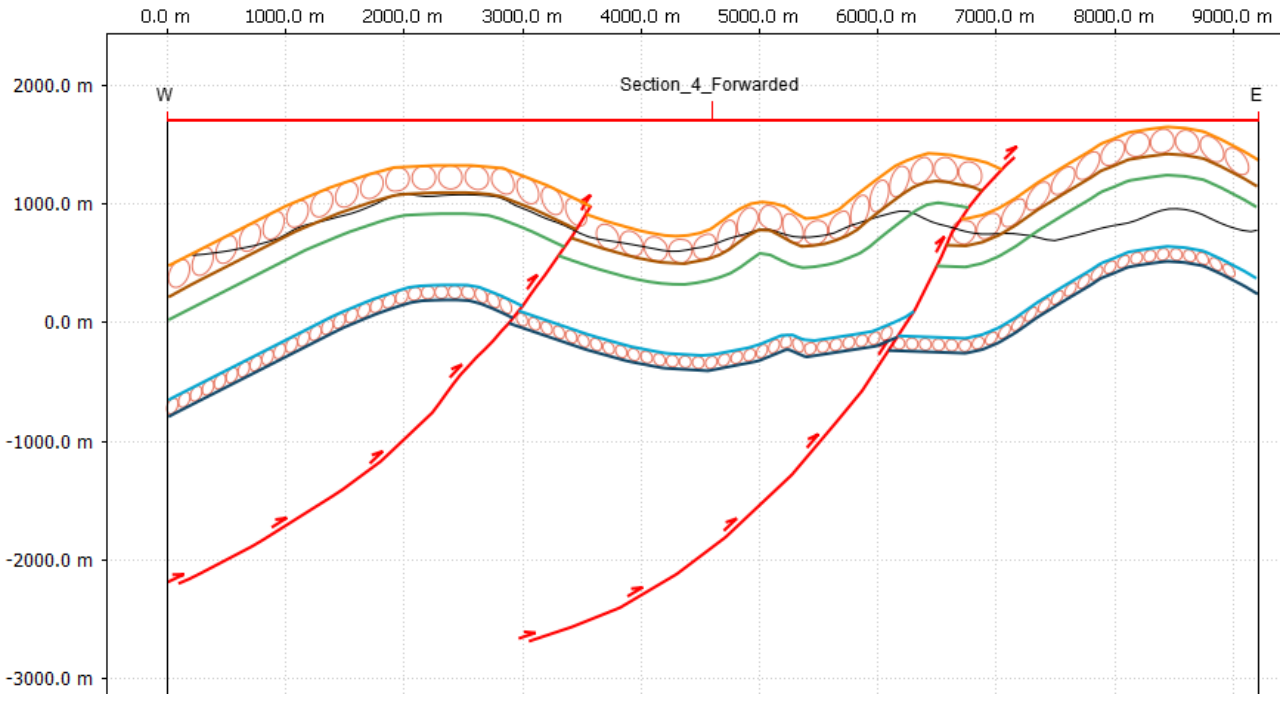

Figure 6.22: Forward model including strain circles

6.3 Shortening

One of the goals of this thesis was to determined how much overall shortening could be measured in the area of interest. This was done by subtracting the present-day E-W width of 9000 m from the measured lengths of the horizon lines in the restored sections (see Figure 6.6, Figure 6.10, Figure 6.14, Figure 6.20). The average horizon lengths from these sections are: Section 1: 11200 m, Section 2: 12700 m, Section 3: 12800 m and Section 4: 10700 m.

Taking the average again results in an average initial length of 11850 m. This implies that the total amount of shortening comes down to 2850 m, which amounts to 24% shortening.

6.3.1 Fault and fold displacement

The amount of displacement along the all faults in the area was measured at each section. The five major faults of this area are the Crupies (C) fault, Les Tonils (LT) fault, Central-East (CE) fault, the Mourelle (M) fault and St. Nazaire (ST) fault. Figure 4.6, Figure 4.7, Figure 4.8 and Figure 4.9 show the locations of the faults in section view and Figure 6.1a shows the location of the faults from above. The displacements are measured from the balanced sections. The displacements are summarized in the table below. Note: the displacement of the CE fault at section 1 is the cumulative displacement of the large CE fault plus the displacement of the smaller branched off fault, see Figure 4.6.

Location		Displacement along fault (m)					Verticale displacement (m)				
		C	M	LT	CE	ST	C	M	LT	CE	ST
North	Sec 1	0	0	250	1250	0	0	0	175	875	0
Middle	Sec 2	300	100	350	1500	300	250	50	300	1200	250
	Sec 3	0	300	400	1500	0	0	275	375	1200	0
South	Sec 4	0	0	100	600	0	0	0	50	300	0

Figure 6.23: Displacement by the C, M, LT, CE and ST faults

Using the Pythagoras equation, the cumulative amount of horizontal displacement due to faulting per section could be calculated. Subtracting the horizontal fault displacement from the total amount of shortening (subsection 6.3), resulted in the displacement due to folding per section. The rounded results are found in Figure 6.24 below.

Location		Horizontal fault displacement (m)	Horizontal fold displacement (m)
North	Sec 1	1070	1780
Middle	Sec 2	1515	1335
	Sec 3	1190	1660
South	Sec 4	600	2250

Figure 6.24: Shortening due to faulting and folding

6.4 Strain observations

The results of forward modelling with strain circles included are shown in Figure 6.16 and Figure 6.22. Section 3 has been forward modelled by making use of the Fold-bend Fold and Flexural Slip algorithms. The large anticline in the middle of Figure 6.16 has been modelled with the fault-bend fold method. Strain circles were added to visualize what kind of deformation resulted from fault-bend folding. The strain circles were all circular before forward modelling commenced. At the forelimb, little deformation has occurred due to fault-bend folding. At the back limb and on top of the anticline, strain circles were deformed into ellipsoids due to angular shear stress.

Section 4 has been forward modelled by using the Flexural Slip Unfolding algorithm, see Figure 6.22. This algorithm was used because it was assumed that at the location of section 4 most deformation was caused by folding. Section 4 seems to show less deformation in general than the fault-bend fold in section 3. Still, some deformation can be observed. Most deformation took place at the fold limbs. Here the circles show an oblique geometry. Little deformation took place on the fold axes.

7 Conclusion & Discussion

7.1 Discussion & Recommendations

Forward modelling wasn't successfully performed on section 1 and 2. This was due to not being able to find a fitting mechanism which could resemble the original interpretations. For future research it is recommended to revise the interpretations for these two sections and try forward modelling again.

Fault propagation folding forms asymmetric folds (Petroleum Experts Ltd., 2019). Asymmetric folds are folds with an oblique geometry. The interpreted sections which can be seen in Figure 6.2, Figure 6.7 and Figure 6.11 show a kind of asymmetric, oblique anticline in the middle. Thus, fault propagation folding could have been a viable structural mechanism to explain these geometries. However, the Fault Propagation Fold algorithm in MOVE could not produce a satisfactory resemblance of the original interpretation. This could be due to a flawed interpretation of the fault geometry, or due to flawed interpretation of the section to start with.

For future research, if going on fieldwork is an option, the results from strain modelling could be verified by taking samples in the field. The researcher should look for natural objects with initial circular geometry, like reduction spots, oolites, conglomerates, breccias, corals, vesicles or pillow lavas (Fossen, 2010). The shape of the field objects could then be compared to the measured deformation in the model.

During this thesis it was assumed that faults have a long, listric geometry. Discussed here are two possible opposing theories for this phenomenon. First, the steep dipping faults aren't thrusts, but oblique strike-slip faults. Some clear evidence of strike slip faulting can be observed just south of the Couspeau area (See Appendix for Dieulefit map). In this scenario, the tectonic model derived in this thesis is false and a new model will be needed. A second theory could be that the faults were originally formed at a lower angle, but rotated to a steeper orientation due to the formation of a younger fault in the footwall.

Additional cross sections could have been constructed for more and better results. Constructing and restoring section is however a very time consuming occupation and the question remains if the sections would have added a significant amount of extra detail.

7.2 Conclusion

The goal for this thesis was to use 2D forward modelling to discover what kind of structural mechanisms were possibly active in the area of interest. Possible mechanisms include fault propagation folding, fault-bend folding and folding without being induced by faulting, or 'regular folding' in short. Fault propagation folding didn't produce any satisfactory outcomes witch could resemble the original interpretations. Fault-bend folding and regular folding did produce a feasible forward model. The large anticline in the middle of Figure 6.15 was modelled by using the Fault Bend Fold algorithm. The model resembles the original interpretation shown in Figure 6.11. Furthermore it was assumed that at the location of section 4, most of the deformation was caused by regular folding. The Flexural Unfolding algorithm was used to forward model Figure 6.21. The model closely resembles the original interpretation shown in Figure 6.17. Therefore it can be concluded that fault-bend folding and regular folding are geological feasible structural mechanisms which have been active in this area.

The secondary goal was to determine how much overall shortening was caused by these mechanisms. By making use of the restored sections, the average total amount of shortening could be calculated. This amounted to be 2850 m, which implies 24% shortening for the whole area. From the total amount of shortening, an average of 38% was caused by faulting, while the other 62% was due to folding.

From the Strain observations it can be concluded that fault-bend folding accumulates little deformation at the forelimb. At the back limb and on top of the folds, strain circles were deformed into ellipsoids due to angular shear stress. The Flexural Slip Unfolding algorithm produces the most deformation at the fold limbs. Little deformation takes place on the fold axes.

8 Acknowledgements

I would like to thank my supervisors Jan Kees Blom, Pierre-Olivier Bruna and Karl-Heinz Wolf for their assistance during this thesis. Even when we couldn't meet in person anymore, Jan Kees and Pierre continued helping me via weekly Zoom and Skype meetings. Their help and feedback was vital for me to be able to do this project. I would like to thank Karl-Heinz for helping me get started with my thesis and for helping to review the final work. A final thanks goes out to Petroleum Experts Ltd for donating the academic licences for the MOVE suite software to the TU Delft.

Bibliography

Amos, C. B., Burbank, D. W., Nobes, D. C., & Read, S. A. L. (2007). Geomorphic constraints on listric thrust faulting: Implications for active deformation in the Mackenzie Basin, South Island, New Zealand. *Journal of Geophysical Research*. doi: 10.1029/2006JB004291

Arnaud, H. (2005). The South-East France Basin (SFB) and its Mesozoic evolution. *Géologie Alpine*.

Bombardiere, L., & Gorin, G. (2000). Stratigraphical and lateral distribution of sedimentary organic matter in Upper Jurassic carbonates of SE France. *Sedimentary Geology*, *132*, 177-203.

Boulila, S., Galbrun, B., Hinnov, L. A., & Collin, P. (2008). High-resolution cyclostratigraphic analysis from magnetic susceptibility in a Lower Kimmeridgian (Upper Jurassic) marl–limestone succession (La Méouge, Vocontian Basin, France). *Sedimentary Geology*, *203*, 54-63.

BRGM. (1969). *Dieulefit geologic map.*

BRGM. (1974). *Die geologic map.*

BRGM. (1975). *Nyons geologic map.*

Bruna, P.-O., Guglielmi, Y., Lamarche, J., Floquet, M., Fournier, F., Sizun, J.-P., ... Hollender, F. (2013). Porosity gain and loss in unconventional reservoirs: Example of rock typing in Lower Cretaceous hemipelagic limestones, SE France (Provence). *Elsevier*. doi: https://doi.org/10.1016/j.marpetgeo.2013.08.008

Caillaud, A., Quijada, M., Huet, B., Reynaud, J. Y., Riboulleau, A., Bout Roumazeilles, V., & Tribovillard, N. (2020). Turbidite induced re oxygenation episodes of the sediment water interface in a diverticulum of the Tethys Ocean during the Oceanic Anoxic Event 1a: The French Vocontian Basin. *The Depositional Record*. doi: https://doi.org/10.1002/dep2.102

Colombié, C., & Strasser, A. (2003). Depositional sequences in the Kimmeridgian of the Vocontian Basin (France) controlled by carbonate export from shallow-water platforms. *Elsevier*, *36*. doi: https://doi.org/10.1016/j.geobios.2003.03.004

De Graciansky, P.-C., & Roberts, D. G. (2011). The Western Alps, from Rift to Passive Margin to Orogenic Belt: An Integrated Geoscience Overview. *Elsevier*.

Dumont, T., Schwartz, S., Guillot, S., Simon-Labric, T., Tricart, P., & Jourdan, S. (2012). Structural and sedimentary records of the Oligocene revolution in the Western Alpine arc. *Journal of Geodynamics*.

Fossen, H. (2010). *Structural geology.* Cambridge University Press.

Föllmi, K. (2012). Early Cretaceous life, climate and anoxia. *Elsevier*.

Föllmi, K., Godet, A., Bodin, S., & Linder, P. (2006). Interactions between environmental change and shallow-water carbonate build-up along the northern Tethyan margin and their impact on the early Cretaceous carbon-isotope record. *Paleoceanography*. doi: https://doi.org/10.1029/2006PA001313

Hallet, D., & Clark-Lowes, D. (2016). Petroleum geology of libya. *Elsevier Science Ltd.*.

Henderson, C. M., Davydov, V. I., Wardlaw, B. R., Gradstein, F. M., & Hammer, O. (2012). The geologic time scale. *Elsevier*. doi: https://doi.org/10.1016/B978-0-444-59425-9.00024-X

Lemoine, M., Bas, T., Arnaud-Vanneau, A., Arnaud, H., Dumont, T., Gidon, M., ... Tricart, P. (1986). The continental margin of the Mesozoic Tethys in the Western Alps. *Marine and Petroleum Geology*.

Li, S., Feng, L., Tang, P., Rao, G., & Bao, Y. (2009). Calculation of depth to detachment and its significance in the Kuqa Depression: A discussion. *Petroleum Science*. doi: 10.1007/s12182-009-0003-2

Nelson, R. A., Patton, T. L., & Serra, S. (1999). *Treatise of Petroleum Geology / Handbook of Petroleum Geology: Exploring for Oil and Gas Traps.* AAPG.

Pei, Y., Paton, D., & Knipe, R. (2014). Defining a 3-dimensional Trishear Parameter Space to Understand the Temporal Evolution of Fault Propagation Folds. *Journal of Structural Geology*. doi: 10.1016/j.jsg.2014.05.018

Petroleum Experts Ltd. (2019). MOVE suite [Computer software]. Retrieved from https://www.petex.com/products/move-suite/

Stampfli, G., & Borel, G. (2002). A plate tectonic model for the Paleozoic and Mesozoic constrained by dynamic plate boundaries and restored synthetic oceanic isochrons. *Earth and Planetary Science Letters.*.

Wan, B., Wu, F., Chen, L., Zhao, L., Liang, X., Xiao, W., & Zhu, R. (2019). Cyclical one-way continental rupture-drift in the Tethyan evolution: Subduction-driven plate tectonics. *Science China Earth Sciences*. doi: https://doi.org/10.1007/s11430-019-9393-4

Watkins, H., Butler, R. W., Bond, C. E., & Healy, D. (2015). Influence of structural position on fracture networks in the Torridon Group, Achnashellach fold and thrust belt, NW Scotland. *Elsevier*.

9 Appendix

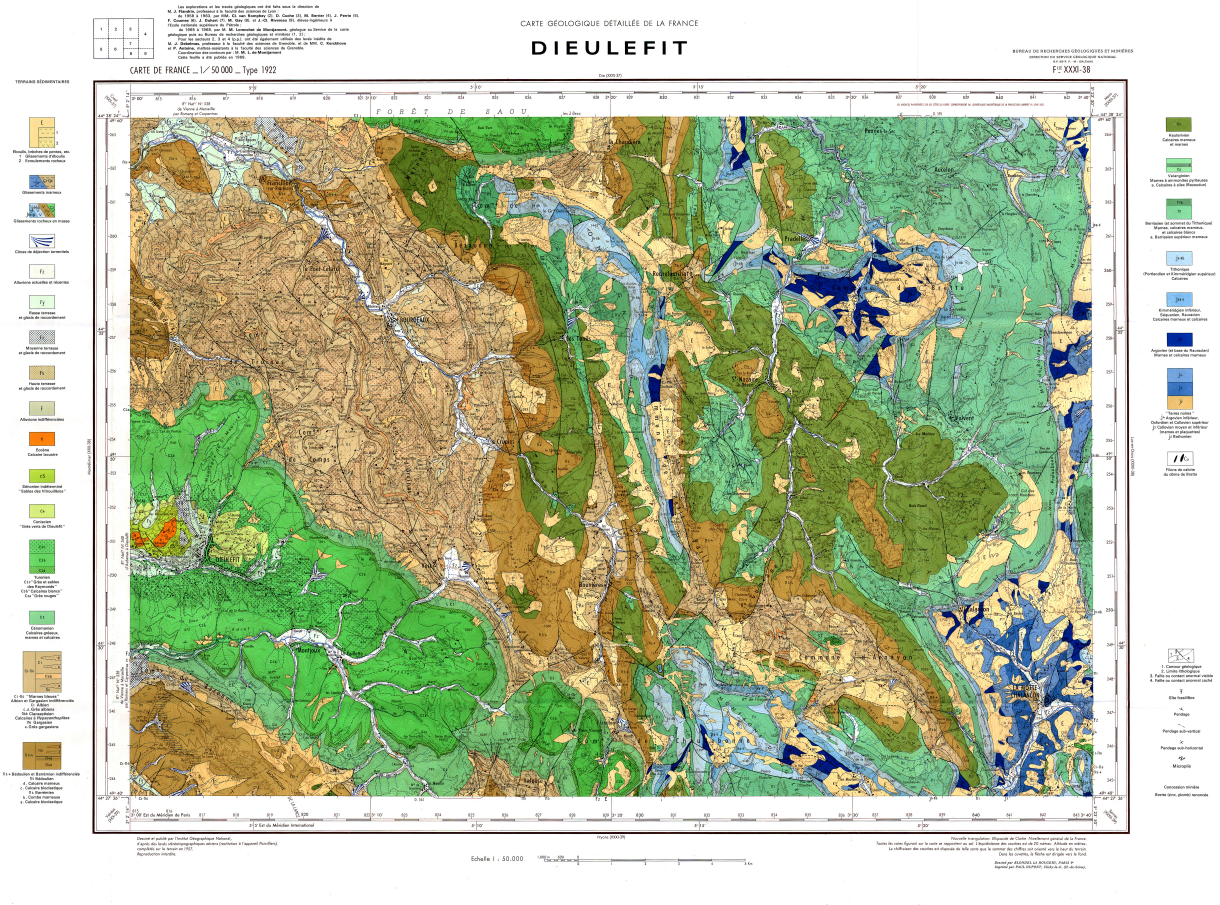

Figure 9.1: Dieulefit geologic map

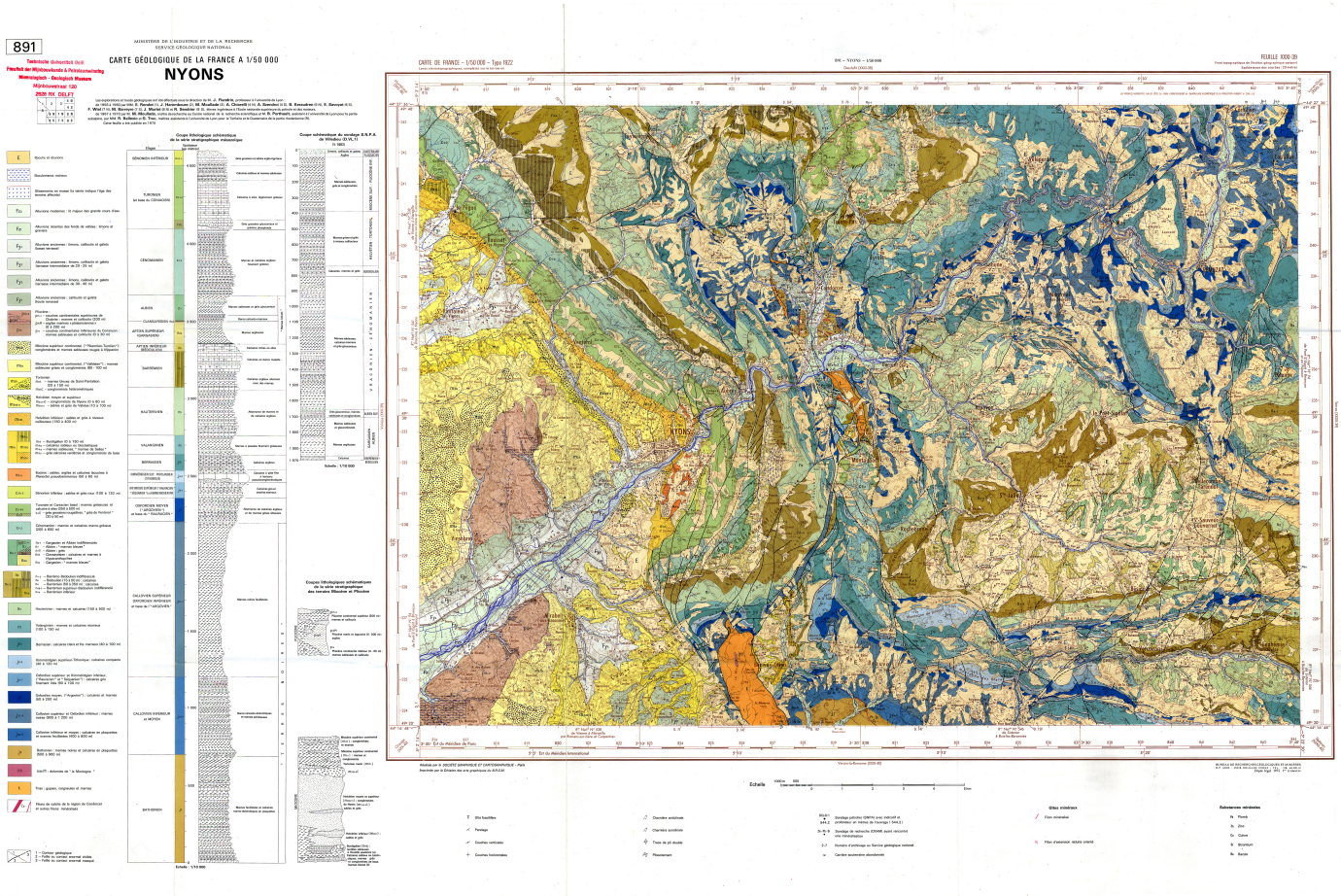

Figure 9.2: Nyons geologic map

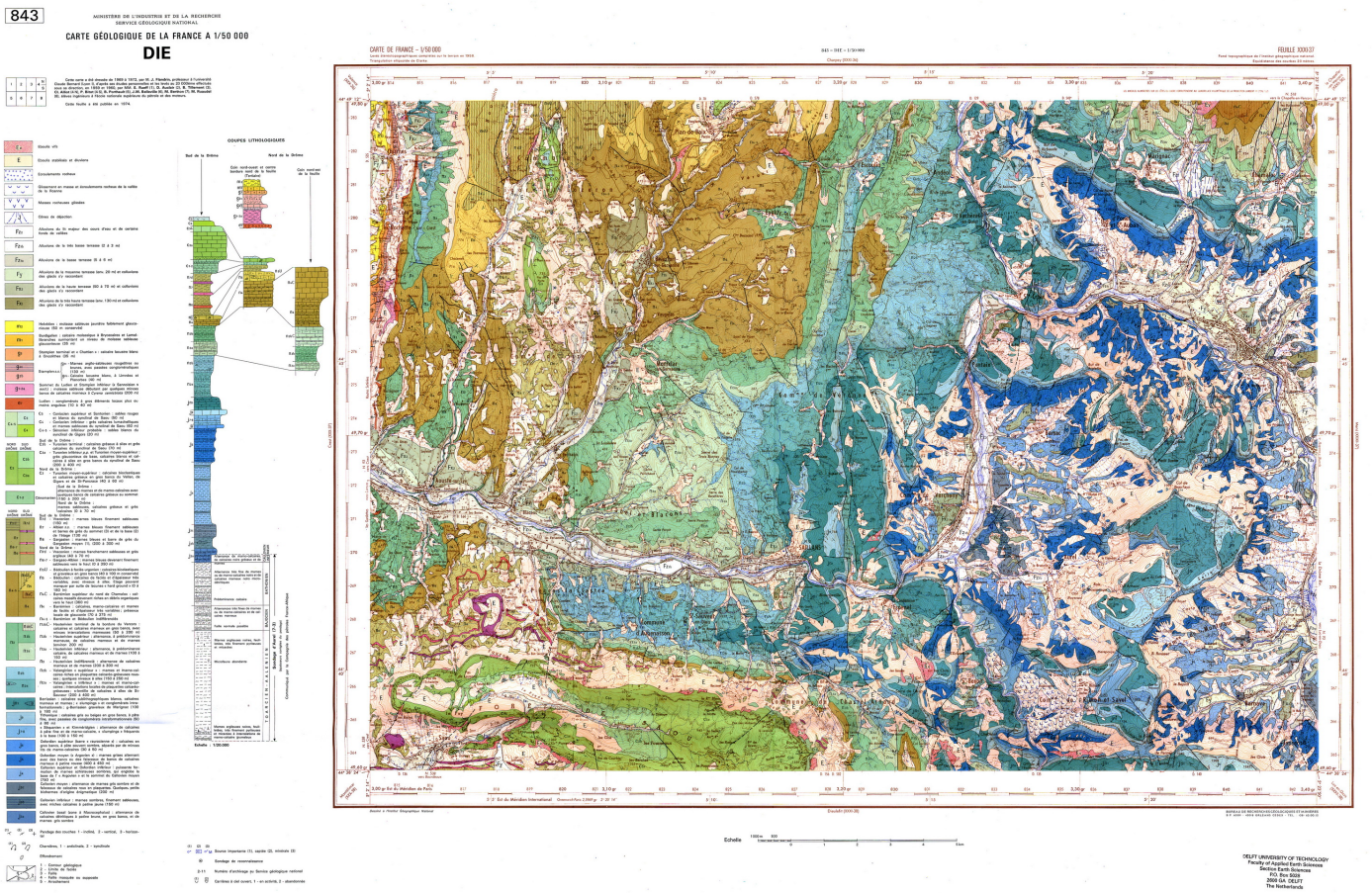

Figure 9.3: Die geologic map